21. Pb AND Sr ISOTOPE AND RARE EARTH ELEMENT COMPOSITION OF SELECTED METALLIFEROUS SEDIMENTS FROM SITES 597 TO 601, DEEP SEA DRILLING PROJECT LEG 92[1]

T. J. Barrett, Department of Geology, University of Toronto
P. N. Taylor, Department of Geology, Oxford University
I. Jarvis, Department of Geology, Kingston Polytechnic
and
J. Lugowski, Department of Geology, University of Toronto[2]

ABSTRACT

Most of the Pb isotope data for the Leg 92 metalliferous sediments (carbonate-free fraction) form approximately linear arrays in the conventional isotopic plots, extending from the middle of the field for mid-ocean ridge basalts (MORB) toward the field for Mn nodules. These arrays are directed closely to the average values of Mn nodules, the composition of which reflects the Pb isotope composition of seawater (Reynolds and Dasch, 1971). Since the Leg 92 samples are almost devoid of continentally derived detritus, it can be inferred that the more radiogenic end-member is seawater. The less radiogenic end-member lies in the very middle of the MORB field, and hence can be considered to reflect the Pb isotope composition of typical ocean-ridge basalt. The array of data lying between these two end-members is most readily interpreted in terms of simple linear mixing of Pb from the two different end-member sources. According to this model, eight samples from Sites 599 to 601 contain 50 to 100% basaltic Pb. Five of these samples have compositions that are identical within the uncertainty of the analyses. We use the average of these five values to define our unradiogenic end-member in the linear mixing model. The ratios used for this average are $^{206}Pb/^{204}Pb = 18.425 \pm 0.010$; $^{207}Pb/^{204}Pb = 15.495 \pm 0.018$; $^{208}Pb/^{204}Pb = 37.879 \pm 0.068$. These values should approximate the average Pb isotope composition of discharging hydrothermal solutions, and therefore also that of the basaltic crust, over the period of time represented by these samples ($\approx$4 m.y., from 4 to 8 Ma).

Sr isotope ratios show a significant range of values, from 0.7082 to 0.7091. The lower ratios are well outside the value of 0.70910 $\pm$ 6 for modern-day seawater (Burke et al., 1982). However, most values correspond very closely to the curve of $^{87}Sr/^{86}Sr$ versus age for seawater, with older samples having progressively lower $^{87}Sr/^{86}Sr$ ratios. The simplest explanation for this progressive reduction is that recrystallization of the abundant biogenic carbonate in the sediments released older seawater Sr which was incorporated into ferromanganiferous phases during diagenesis.

Leg 92 metalliferous sediments have total rare earth element (REE) contents that range on a carbonate-free basis from 131 to 301 ppm, with a clustering between 167 and 222 ppm. The patterns have strong negative Ce anomalies. Samples from Sites 599 to 601 display a slight but distinct enrichment in the heavy REE relative to the light REE, whereas those from Sites 597 to 598 show almost no heavy REE enrichment. The former patterns (those for Sites 599 to 601) are interpreted as indicating moderate diagenetic alteration of metalliferous sediments originating at the EPR axis; the latter reflect more complete diagenetic modification.

INTRODUCTION

It has been known for some time that sediments near the East Pacific Rise (EPR) are strongly enriched in Fe, Mn, and other transition metals by comparison with normal pelagic sediments (Murray and Renard, 1891; Revelle, 1944; Boström and Peterson, 1966; Boström et al., 1969; Bender et al., 1971). It is generally accepted that these metals were leached from the basaltic crust by seawater hydrothermal systems and/or subsequently scavenged from seawater by authigenic Fe–Mn precipitates which formed upon hydrothermal discharge and settled onto the ocean floor (Corliss, 1971; Bonatti et al., 1972; Dymond et al., 1973; Piper, 1973; Bonatti, 1975; Dymond and Veeh, 1975; Cronan, 1980; Dymond, 1981; Thompson, 1983). Studies of the mineralogy, geochemistry, and origin of metalliferous sediments in the eastern Pacific (Fig. 1) have concentrated on the recent sediments of the EPR (Sayles and Bischoff, 1973; Heath and Dymond, 1977, 1981; Lyle, 1981; Marchig and Gundlach, 1982; Marchig et al., 1982), the Bauer Deep (Sayles et al., 1975; Dymond and Veeh, 1975; Dymond, 1981; McMurtry et al., 1981; Lyle, 1981; Field et al., 1981), and the Galapagos Hydrothermal Mounds Field (Corliss et al., 1978; Hekinian et al., 1978; Williams et al., 1979; Varnavas et al., 1983; Honnorez, Von Herzen, et al., 1983; Honnorez, Von Herzen, Barrett, et al., 1981; Barrett and Friedrichsen, 1982; Moorby, 1983).

Fewer geochemical data are available on the ancient analogs of these deposits, which have been cored by the Deep Sea Drilling Project both to the east and to the west of the EPR. Metalliferous sediments of Eocene–Oligocene age have been recovered from the central Pacific at the base of the sediment column at DSDP Sites 74 and 75 (Tracey et al., 1971; von der Borch et al., 1971), 77 and 78 (Hays et al., 1972), and 159, 160, and

[1] Leinen, M., Rea, D. K., et al., *Init. Repts. DSDP*, 92: Washington (U.S. Govt. Printing Office).

[2] Addresses: (Barrett, Lugowski) Department of Geology, University of Toronto, Toronto, Ontario, Canada M5S 1A1; (Taylor) Department of Geology, Oxford University, Oxford, Great Britain OX1 3PR; (Jarvis) Department of Geology, Kingston Polytechnic, Kingston-upon-Thames, Great Britain KT1 2EE.

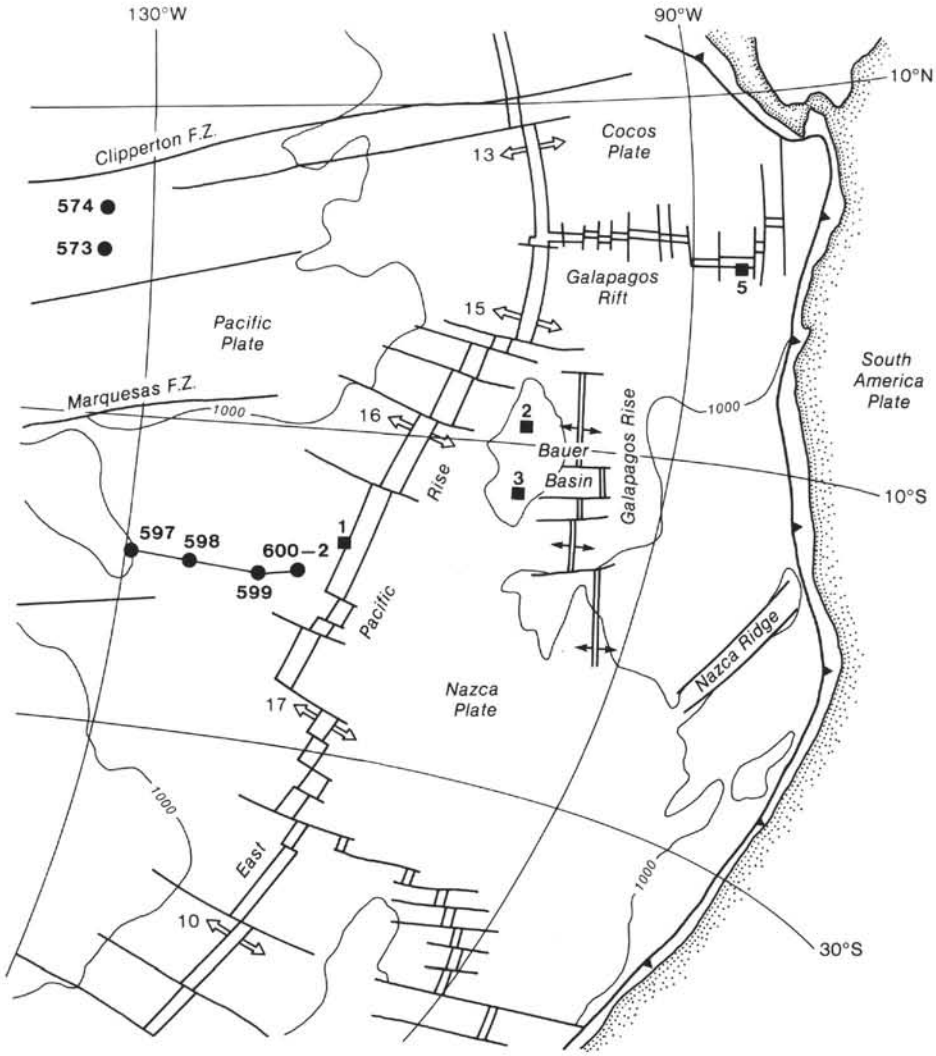

Figure 1. Index map of the eastern Pacific showing the locations of Leg 92 Sites 597 to 602 (the East Pacific Rise transect), together with DSDP Sites 573 and 574 on the Pacific Plate. Also shown are the locations of various metalliferous sediments. Numbers 1 to 3 are referenced in Fig. 5; number 5 gives location of Galapagos hydrothermal mounds (Honnorez et al., 1981). Numbers next to white arrows flanking the East Pacific Rise give relative divergent plate motion in cm/yr. These values and base map are from the plate-tectonic map of the circum-Pacific region (Am. Assoc. Pet. Geol., 1982). Most of the samples in Dasch's (1981) Pb isotope study (as plotted in Fig. 5) are from the area of the Nazca Plate lying between 6° and 21°S, and 93° and 115°W.

162 (van Andel, Heath, et al., 1973; Cronan, 1973). Miocene metalliferous sediments occur at the base of Site 81 (Hays et al., 1972) and in the upper part of the sediment column at Sites 74 (von der Borch et al., 1971) and 159 (Cronan, 1973). The most recent studies of these deposits are those of Cronan (1973, 1976), Cronan and Garrett (1973), and Leinen (1981), who described similar material from the northeastern Pacific. In the eastern Pacific, Miocene metalliferous sediments also have been recovered at Site 319, which is located in the Bauer Basin on the Nazca Plate (Yeats, Hart, et al., 1976). Very recently, Eocene–Oligocene metalliferous sediments were recovered at Sites 573 and 574, Leg 85, in the equatorial eastern Pacific (Mayer et al., 1982).

DSDP Leg 92 drilled at four sites along an east–west transect at 19°S which intersected basement ranging in age from Oligocene to Pliocene (about 28 to 5 Ma). Nearly complete recovery of the overlying sediment was achieved through use of piston coring techniques. The cores recovered by Leg 92 make it possible to study how sediment composition and geochemistry are affected by (1) lateral distance from the East Pacific Rise hydrothermal systems and (2) downhole distance (i.e., age) at a particular site. The Leg 92 sites, as well as the Leg 85 sites which lie about 20° latitude (≈2000 km) to the north, were generated at the EPR and are presently located near the eastern margin of the Pacific Plate. (Site 597 was apparently formed at the Mendoza Rise, the forerunner of the present EPR.)

METHODS AND MATERIALS

Methods

All samples were prepared in the manner described in the Appendix. All isotopic and REE analyses are on residues following removal

of the carbonate phase with an acid leach; that is, they are on a carbonate-free basis. For some samples the initial residue was further treated with a second leach, then analyzed again. For a given sample, the residue after the first leach and the residue after the second leach are referred to by numbers *(1)* and *(2)*, respectively, in Tables 1 and 2. Pb and Sr concentrations in Table 1B are also for the carbonate-free fraction, but represent the total soluble Pb and Sr present in the second and third leachates (see Appendix). Hence, they do not include the small percentage of insoluble material (usually $<7\%$ of the carbonate-free fraction) remaining after these leaches, and therefore should contain only the metalliferous component of the sediment. The insoluble material was present, however, in the samples subjected to isotopic and REE analyses, as these were performed on initially solid residues, not leachates.

Removal of the carbonate fraction increases the relative abundance of such elements as Pb and the rare earths, thereby facilitating their analysis, particularly if the element concentrations were near the limits of detection prior to carbonate removal. (Because of the high Sr concentration in carbonate shells, Sr contents are actually decreased by the removal of the carbonate fraction; however, sufficient Sr still remains for analytical purposes.) Comparisons between the carbonate content and the percentage of Ca in pelagic sediments from the eastern Pacific (Sayles et al., 1975; Dymond et al., 1976) have shown that $<2\%$ CaO occurs in the noncarbonate fraction. Other elements in untreated sediments (with the notable exception of Sr) vary inversely with Ca, indicating that although calcium carbonate acts as a dilutant in sediments, it does not control the distribution of minor and trace elements.

The mineralogies of selected carbonate-free samples were determined by X-ray diffraction (XRD) at the Institute of Oceanographic Sciences, Godalming, U.K. Powders were reground in a tungsten-carbide tema to minimize grain-size variations between samples, and mounted in random aggregate cavity mounts. Analyses were performed using CuK_α radiation at 40 kV/20 mA and a Philips PW 1050 goniometer with AMR monochromator. Scan speeds of 0.25° 2Θ/min. were used throughout.

For Pb analysis, sample splits of carbonate-free powders were digested in HF using autoclave bombs. Pb was separated by loading the sample onto anion exchange resin columns in HBr, washing the column with HBr, and then eluting Pb in water. Samples were loaded onto single Re filaments with orthophosphoric acid and silica gel, and analyzed on a VG Isomass 54E thermal ionization mass spectrometer at Oxford. Pb isotope data have been corrected for mass fractionation of -0.1% per AMU. Typical uncertainties in the Pb isotope ratios are 0.1% (2σ).

Sr was extracted from splits of carbonate-free sample powders by standard ion-exchange methods (cf. O'Nions and Pankhurst, 1973) and analyzed on the VG Isomass 54E mass spectrometer at Oxford. $^{87}Sr/^{86}Sr$ ratios have been normalized to a value of 0.70800 for the Eimer and Amend Sr standard (measured value = 0.07801). Typical errors on $^{87}Sr/^{86}Sr$ measurements are 0.01%. Pb and Sr concentrations were determined by atomic absorption spectrophotometry in a manner identical to that of the Leg 92 sediment standard (Appendix). Reproducibility of results was better than $\pm 5\%$.

The rare earth elements and Y were extracted from splits of carbonate-free powders following $HF-HClO_4$ open digestion using a cation separation procedure modified from Walsh et al. (1981) and Thompson and Walsh (1983). La, Ce, Pr, Nd, Sm, Eu, Gd, Dy, Ho, Er, Yb, Lu, and Y were determined simultaneously using a Philips PV 8210 inductively coupled plasma (ICP) at the Department of Geology, Kings College, London. Calibration curves were constructed by using artificial composite standards (made from BDH and Eldrich standard solutions for atomic absorption, and Specpure chemicals), calculated to match closely the range of values expected for each element in the unknowns. Careful matching of matrices is essential to minimize interference effects. Raw intensity data were processed on a Digital PDP 11-34 computer utilizing a program developed by I. Jarvis which incorporates drift and blank correction. The REE data were additionally corrected for interelement interferences by Ba, Ca, Sr, Ti, and Zr to compensate for the small proportion of these elements which remain after the cation exchange procedure. Analytical precision as determined by replicate analyses is better than $\pm 3\%$ for all of the REE present in amounts >0.2 ppm. By reference to international standards, absolute accuracy is judged to be better than $\pm 5\%$ of the quoted values (Walsh et al., 1981; Jarvis and Jarvis, 1985).

Materials

Samples for REE and isotope analysis were selected from a larger sample set taken at approximately 1.5-m intervals throughout the length of the cores. Sediment lithology and stratigraphic locations of the analyzed samples for the various sites are shown in Figure 2. The majority of the sediment sequence is upper Oligocene–Miocene at Site 597, Miocene at Sites 598 and 599, and Pliocene–Pleistocene at Sites 600 and 601. All of these sediments are essentially light-colored calcareous nannofossil oozes with varying admixtures (commonly 20 to 40%) of a darker, fine-grained metalliferous component. Onboard smear slide examination revealed this latter component to consist of Fe oxides and hydroxides, RSO (red brown to yellow brown semiopaque oxides), and poorly crystalline clays. It should be noted, however, that although the stratigraphic columns (based on shipboard study) in Figure 2 give the main sediment lithology as clayey nannofossil ooze, XRD data indicate that the clay component in the noncarbonate fraction of the samples we analyzed was insignificant relative to the oxide–oxyhydroxide component.

Variations in the proportion of this latter component determine the color of the sediment, which ranges from light-colored through yellow brown to brown and even very dark brown. Sedimentological features at each site are summarized in the individual site chapters (this volume).

RESULTS

Mineralogy

Preliminary mineralogical analysis of the Leg 92 samples by X-ray diffraction (XRD), following removal of the carbonate phase, indicates that the dominant phase is moderately to well-crystallized goethite, with lesser and varying proportions of apatite (carbonate–fluorapatite), and in some samples minor quartz (Fig. 3). A few samples contain distinct enrichments of phillipsite. When samples are treated with a second acid leach, which preferentially dissolves amorphous and/or poorly crystallized oxyhydroxide phases, the goethite peaks become somewhat higher and sharper, and some of the apatite (where this mineral is XRD detectable) is also removed. Although removal of some apatite may be a factor in increasing the definition of the goethite peaks, the increased definition also occurs in samples lacking detectable amounts of apatite. In such samples, the second acid leach is presumably removing poorly crystallized goethite (and possible X-ray amorphous material), leaving behind only the well-crystallized goethite.

Pelagic sediments in other areas of the eastern Pacific are composed dominantly of calcium carbonate (low-Mg calcite), biogenic opal, and clay minerals. Common accessory phases include quartz, feldspar, barite, biogenic apatite (fish debris), zeolites (phillipsite, clinoptilolite), and volcanic glass. Metalliferous sediments typically contain some of these components admixed with varying proportions of ferromanganese material. The ferromanganese phase was initially regarded as being X-ray amorphous (Boström and Peterson, 1966; Boström et al., 1969; von der Borch and Rex, 1970; von der Borch et al., 1971; Bender et al., 1971), but ultra-slow-scan XRD and other techniques have shown that a number of discrete mineral phases may be recognized (Dasch et al., 1971; Dymond et al., 1973; Sayles and Bischoff, 1973; Sayles et al., 1975; Heath and Dymond, 1977; Dymond and Eklund, 1978). Authigenic, brownish Fe-smectite (generally identified as Fe-montmorillonite) is an impor-

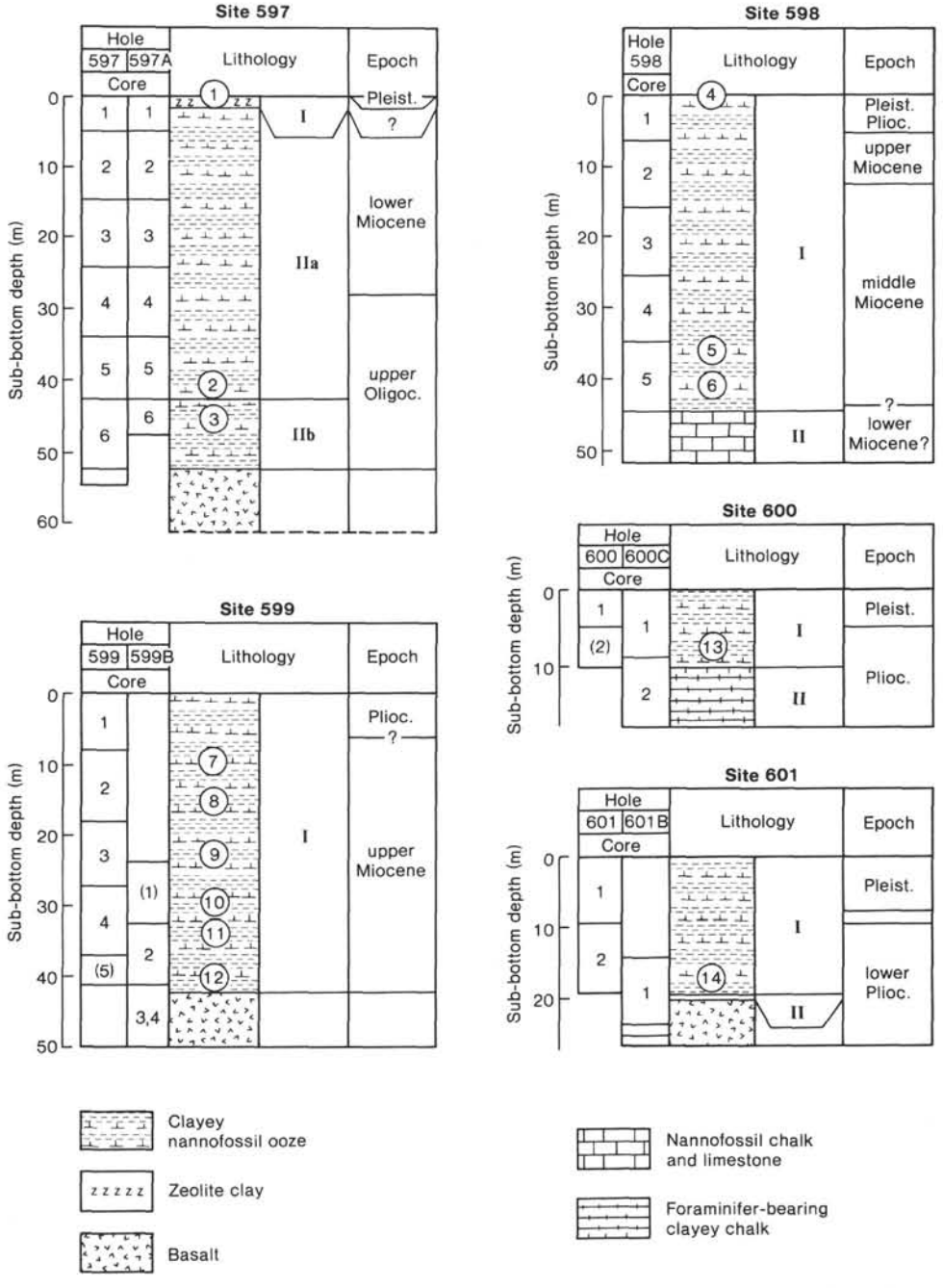

Figure 2. Stratigraphic summary of sediments drilled at DSDP Sites 597 to 601, Leg 92. Locations of samples analyzed in this study are shown by the circled numbers in the stratigraphic columns. The sample numbers are keyed to DSDP sample numbers (which include within-section cm intervals) in Table 1. Table 1 also gives age ranges for the samples. The lithologic units at each site are described in detail in the site chapters. Note that the clay component in the noncarbonate fraction of the samples is dominantly Fe- and Mn-rich oxide-oxyhydroxide.

tant constituent of recent pelagic clays throughout the eastern and central Pacific (Aoki et al., 1974; Hein et al., 1979). Nontronite (a yellow green aluminum-poor Fe-smectite) is the major iron-bearing phase in the Galapogos Hydrothermal Mounds (Honnorez, Von Herzen, Barrett, et al., 1981; Honnorez, Von Herzen, et al., 1983). Other minerals identified in metalliferous sediments include goethite (the dominant phase in basal deposits intersected by some DSDP holes) and the manganiferous phases psilomelane, ∂MnO_2, birnessite, and todorokite. Except for goethite, none of the above minerals was detected by XRD in the samples analyzed in the present study. In particular, no Fe-smectite was observed, even though this is the dominant metalliferous phase in the claystones at the Leg 85 sites, only 200 km to the north (Jarvis, 1985). This result is not a consequence of different analytical techniques, because the Leg 92 sediments were investigated by using the same instrument

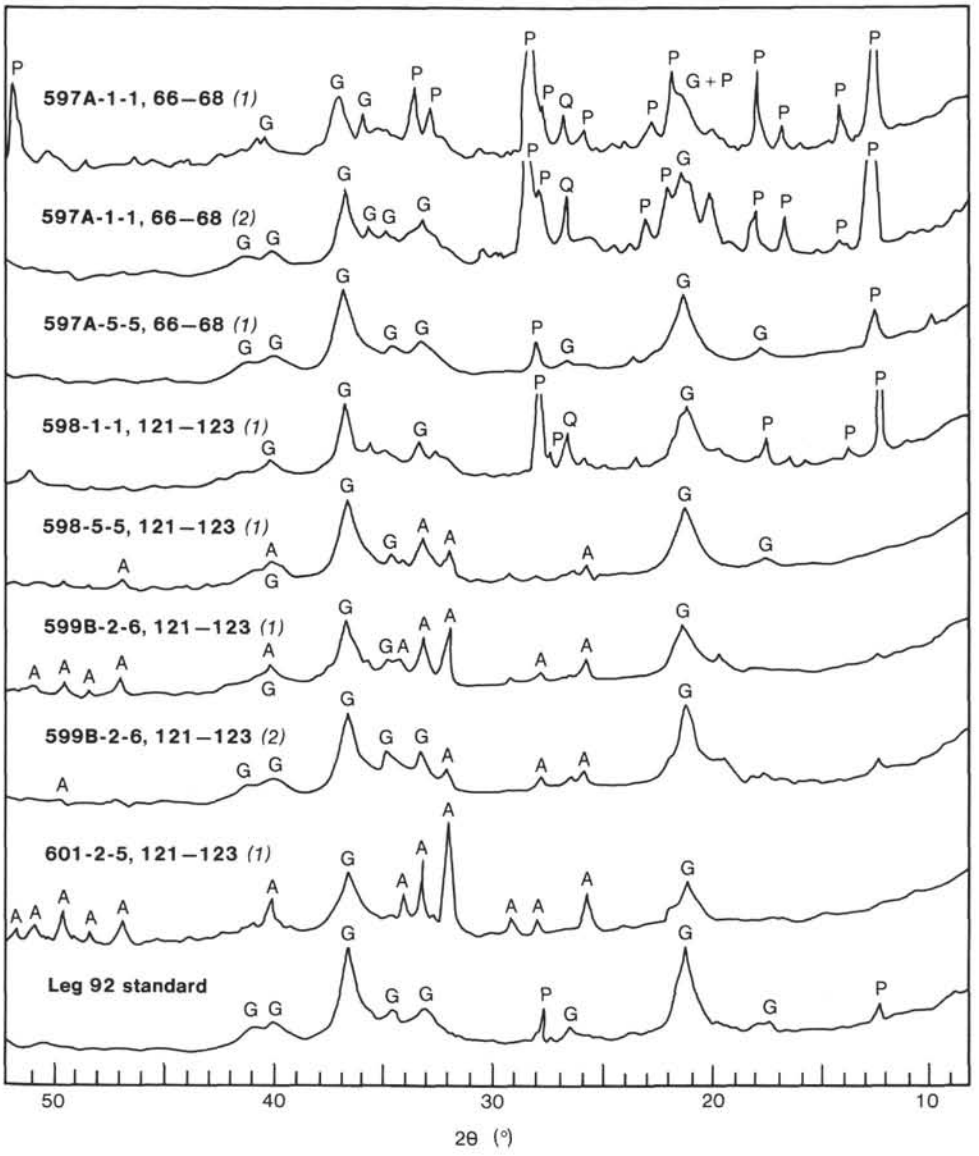

Figure 3. X-ray diffraction traces of selected sediment samples, DSDP Leg 92. Samples followed by *(1)* have been leached with acetic acid to remove the carbonate fraction. Samples followed by *(2)* have been leached a second time to remove amorphous to poorly crystalline phases. Minerals detected: G = goethite; P = phillipsite; A = apatite; Q = quartz. All samples were run at 0.25° 2θ/min. Diffractograms of other samples (listed in Table 1) display the same mineralogical features as those shown.

and the same analytical procedures as were used for the Leg 85 sediments.

Pb and Sr Isotopes

Pb Isotopes

Pb isotope ratios for the sediment samples are listed in Table 1A, which also gives the Sr isotope compositions of the sample splits. Sample numbers followed by *(1)* indicate that the analysis is for the carbonate-free fraction; those followed by *(2)* have been subjected to a second leach to remove amorphous and poorly crystalline compounds. Table 1B gives Pb and Sr concentration data for five samples that were treated with both the first and second leaches. The Pb isotope data are plotted in Figures 4 and 5. In Figure 4, the compositional fields for oceanic Mn nodules (Reynolds and Dasch, 1971), mid-ocean ridge basalts or MORBs (Sun, 1973), and basalts from spreading axes in the northeast Pacific (Church and Tatsumoto, 1975) are also shown for comparison. Most of the Pb data for the Leg 92 metalliferous sediments form approximately linear arrays in the two isotopic plots; the arrays extend from the middle of the MORB field toward the Mn nodule field (two samples which plot to the right of the arrays are discussed later). These arrays are directed toward the average values of Mn nodules, the composition of which reflects the Pb isotope composition of seawater (Reynolds and Dasch, 1971), which in turn is very similar to the average value of oceanic sediment (Stacey and Kramers, 1975). Since the Leg 92 samples are nearly devoid of continentally derived detritus, it can be assumed that the more

Table 1A. Pb and Sr isotope composition for selected samples from Sites 597 to 601, DSDP Leg 92.

DSDP sample number (interval in cm)	Age bracket (m.y.)	Sample number in Figs. 2, 4, 5[a]	$^{206}Pb/^{204}Pb$	$^{207}Pb/^{204}Pb$	$^{208}Pb/^{204}Pb$	$^{87}Sr/^{86}Sr$
597A-1-1 (66–68)	0–14.2	1 *(1)*	18.676	15.569	38.407	0.70892
		1 *(2)*[b]	18.684	15.578	38.444	0.70812
597A-5-5 (66–68)	24.8–28.3	2 *(1)*	18.789	15.513	38.270	0.70824
597-6-2 (66–70)	24.8–28.3	3 *(1)*	18.825	15.538	38.356	0.70827
		3 *(2)*	18.847	15.558	38.449	0.70655
598-1-1 (121–123)	1.9–5.4	4 *(1)*	18.656	15.575	38.404	0.70893
598-5-1 (121–123)	14.2–17.0	5 *(1)*	18.575	15.538	38.070	0.70959[c]
		5 *(2)*	18.556	15.527	38.045	0.70890
598-5-5 (121–123)	14.2–17.0	6 *(1)*				0.70891
599-2-2 (121–123)	3.7–5.4	7 *(1)*	18.425	15.496	37.864	0.70901
		7 *(2)*	18.420	15.487	37.822	0.70887
599-2-6 (121–123)	5.4–6.7	8 *(1)*	18.416	15.481	37.820	0.70900
		8 *(2)*	18.397	15.484	37.812	0.70895
599-3-4 (121–123)	5.4–6.7	9 *(1)*	18.467	15.522	37.895	0.70899
599-4-2 (121–123)	5.4–6.7	10 *(1)*				0.70901[d]
		10 *(2)*				0.70887
599-4-5 (121–123	6.7–8.1	11 *(1)*	18.422	15.502	37.867	0.70901
599B-2-6 (121–123)	6.7–8.1	12 *(1)*	18.569	15.560	38.099	0.70898
600C-1-5 (121–123)	3.7–4.6	13 *(1)*	18.435	15.513	37.947	0.70907
		13 *(2)*	18.415	15.480	37.854	0.70909
601-2-5 (121–123)	3.7–4.6	14 *(1)*	18.426	15.483	37.897	0.70904

[a] Sample numbers followed by *(1)* have been treated with one acid leach to remove the carbonate fraction; those followed by *(2)* have also been subjected to a second leach to remove amorphous and poorly crystalline phases. All data given on a salt-free basis.

[b] Duplicate values: $^{206}Pb/^{204}Pb$ = 18.681; $^{207}Pb/^{204}Pb$ = 15.578; $^{208}Pb/^{204}Pb$ = 38.450.

[c] Duplicate value = 0.70963.

[d] Duplicate value = 0.70897.

Table 1B. Pb and Sr concentrations and mass accumulation rates for selected samples from Sites 597 to 601, DSDP Leg 92.

DSDP Sample number (interval in cm)	Sample number in Figs. 2, 4, 5	Pb concentration (ppm)		Sr concentration (ppm)		Mass accumulation rate in bulk sediment (mg/[cm^2 × 10^3 yr.])	
		Bulk sediment	Carbonate-free fraction	Bulk sediment	Carbonate-free fraction	Pb	Sr
598-5-1 (121–123)	5 *(1)*	49.7	240	87.1	418	0.0269	0.0472
	5 *(2)*	32.5	158	2.5	12		
599-2-2 (121–123)	7 *(1)*	60.2	220	98.1	367	0.0288	0.047
	7 *(2)*	42.5	156	7.7	35.4		
599-4-2 (121–123)	10 *(1)*	67.4	207	132	407	0.0443	0.0867
	10 *(2)*	47.5	147	11.5	35.4		
599B-2-6 (121–123)	12 *(1)*	82.2	181	175	385	0.054	0.115
	12 *(2)*	54.5	120	19.1	42.1		
600C-1-5 (121–123)	13 *(1)*	72.7	251	125	429	0.0744	0.128
	13 *(2)*	52.5	182	8.1	27.7		

Note: All data are given on a salt-free, insoluble-residue-free basis. *(1)* and *(2)* as defined for Table 1A. Pb and Sr concentrations are based on the total soluble Pb and Sr present in the second and third leachates—see Appendix. Therefore Pb and Sr concentrations, and their mass accumulation rates, do not include the small percentage of insoluble material (usually <7%) remaining after the second and third leaches. (Such material was present in the samples subjected to isotopic and REE analyses.) Bulk sediment values were derived from the carbonate-free values, using the known carbonate contents of the salt-free sediment. The mass accumulation rates were calculated using sediment accumulation rates determined for the various cored intervals (see site chapters).

radiogenic end-member is seawater (as given by the average Pb isotope composition of Mn nodules). A cluster of our data lies in the middle of the MORB field, indicating that the less radiogenic end-member of the arrays has a Pb isotope composition typical of oceanic tholeiite. The array of data lying between these two end-members is most readily interpreted in terms of the simple linear mixing of Pb from the two different end-member sources.

Although the data are limited, Figure 4 suggests a compositional difference between the relatively radiogenic sediments from Sites 597 and 598 and the significantly less radiogenic sediments from Sites 599 to 601. According to the linear mixing model, the eight samples from Sites 599 to 601 contain 50 to 100% basaltic Pb. All of these samples are of very similar age (3.7 to 8.1 m.y.); hence, age-related effects during diagenesis are unlikely to have caused the variations present in the percentage of basaltic Pb. As an explanation we prefer variations in the degree of hydrothermal activity on the EPR; this may cause different proportions of basaltic Pb to be discharged into the overlying water column at different times. Pre-

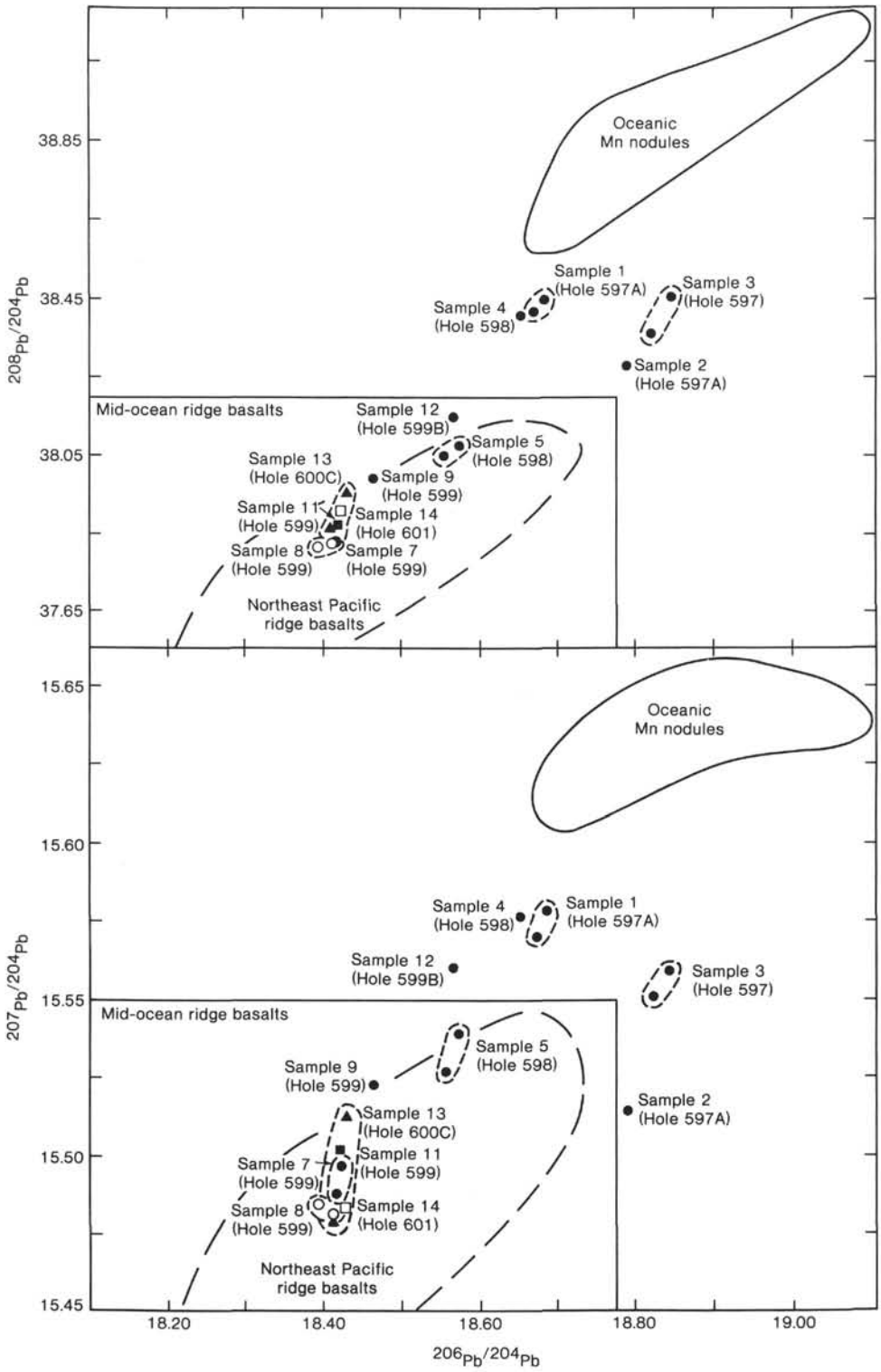

Figure 4. $^{208}Pb/^{204}Pb$ and $^{207}Pb/^{204}Pb$ vs. $^{206}Pb/^{204}Pb$ for sediments from DSDP Sites 597 to 601 (carbonate-free basis). Single data points represent the results after the first leach (carbonate removed). Data pairs encircled by a dashed line are values after first and second leaches. Isotope data are given in Table 1A. The fields for oceanic Mn nodules are from Reynolds and Dasch (1971), those for mid-ocean ridge basalts are from Sun (1973), and those for northeast Pacific ridge basalts are from Church and Tatsumoto (1975).

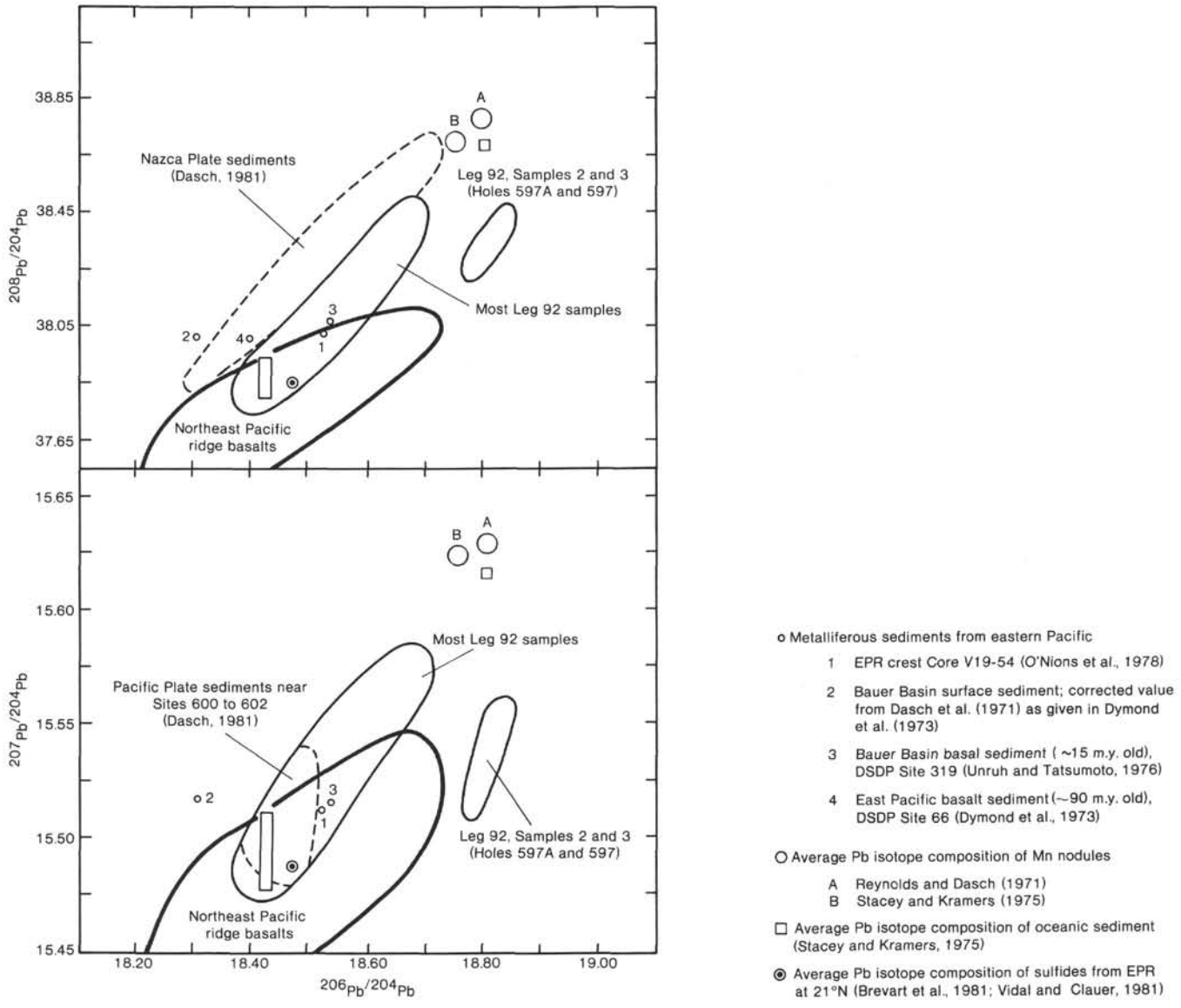

Figure 5. $^{208}Pb/^{204}Pb$ and $^{207}Pb/^{204}Pb$ vs. $^{206}Pb/^{204}Pb$ for sediments of the Pacific Plate recovered at DSDP Sites 597 to 601 (carbonate-free basis). Average composition of the least radiogenic end-member for the Leg 92 sediments is shown by open rectangles. Also shown are four other metalliferous sediments from the eastern Pacific; average Pb isotope composition of Mn nodules and average oceanic sediment; Dasch's (1981) Pb isotope data for Nazca Plate metalliferous surface sediments (upper diagram); Dasch's (1981) Pb isotope data for the eastern edge of the Pacific Plate (lower diagram); and average Pb isotope composition of sulfides from the EPR at 21°N (Brevart et al., 1981; Vidal and Clauer, 1981).

sumably, periods of intense discharge result in a higher ratio of basaltic to seawater Pb in the colloidal precipitates which form upon discharge.

Five of the eight samples mentioned above (numbers 7, 8, 11, 13, and 14) have compositions that are identical within the uncertainty of analysis. We use the average of these five values to define our unradiogenic end-member in the linear mixing model (Fig. 5). The ratios for this average are: $^{206}Pb/^{204}Pb = 18.425 \pm 0.010$; $^{207}Pb/^{204}Pb = 15.495 \pm 0.018$; $^{208}Pb/^{204}Pb = 37.879 \pm 0.068$. These values lie in the center of Sun's (1973) field for MORBs. Our end-member value for the metalliferous sediments from Sites 599 to 601 should approximate the average Pb isotope composition of discharging hydrothermal solutions over the period of time represented by these samples ($\approx$4 m.y., from 4 to 8 Ma). These solutions in turn approximate the average Pb isotope composition of the upper oceanic crust at 19°S during that time interval. The end-member value is in fact very close to the average value for tholeiites (29 samples) from the Gorda and Juan de Fuca ridges in the northeast Pacific: $^{206}Pb/^{204}Pb = 18.460$; $^{207}Pb/^{204}Pb = 15.479$; $^{208}Pb/^{204}Pb = 37.886$ (Church and Tatsumoto, 1975), and to an average value for 13 selected samples from Pacific Ocean ridges (some taken from Church and Tatsumoto, 1975) given by Zindler et al. (1982): $^{206}Pb/^{204}Pb = 18.355$; $^{207}Pb/^{204}Pb = 15.477$; $^{208}Pb/^{204}Pb = 37.838$. Unruh and Tatsumoto (1976) also report a Pb isotope composition for a sample of basal metalliferous sediment from DSDP Site 319 (Fig. 5) which plots near the middle of their array of values for the underlying basalts at that site.

Also shown in Figure 5 is the average Pb isotope composition of metal sulfides forming directly from discharging 350°C solutions on the EPR axis at 21°N (Vidal and Clauer, 1981; Brevart et al., 1981). This value is very close to our unradiogenic end-member composition. Hence, it appears that although hydrothermal solutions must lose some of their basaltic Pb to directly precipitated sulfides (at and/or below the seawater interface), sufficient Pb emanates into seawater to produce metalliferous sediments that can closely match the Pb isotope compositions of both the axial sulfide deposits and the basaltic crust. Some of the emanating Pb may be in the form of fine metal sulfide particulate matter (as in "black smokers"), whereas some may be in dissolved form. In the former case, reaction with seawater probably produces oxidized particles quite rapidly; in the latter, the dissolved Pb is either coprecipitated with or absorbed onto colloidal Fe-Mn-rich hydroxyoxide precipitates. In both cases, lateral transport of the fine particulate material by ocean bottom currents is believed to be the means by which the basaltic Pb is distributed to sediments far removed from the ridge axis (see below).

The three Site 597 samples have the most radiogenic values, whereas of the two Site 598 samples, one displays a radiogenic value and one is intermediate between the radiogenic group and the group from Sites 599 to 601 (Fig. 4). It is worth noting that the two surficial samples from Sites 597 and 598 (Samples 1 and 4) have virtually identical compositions. In terms of the linear mixing model, the ratio of seawater to basaltic Pb in these two samples would be about 5 to 1. This ratio implies that even at distances of greater than 700 km west of the EPR axis, a small component of basaltic Pb is present in the sediments. By contrast, the Pb in surficial samples from the Bauer Basin, located some 700 km east of the EPR, is dominantly basaltic (Dasch et al., 1971; Unruh and Tatsumoto, 1976). Although more data on surficial samples from west of the EPR are obviously required, it may be that differences in ocean bottom current circulation on either side of the EPR are responsible for differences in the degree to which basaltic Pb, in association with the colloidal precipitates, is transported laterally (away from the ridge axis).

Samples 2 and 3 lie slightly to the right of the trend established by the other samples (Fig. 5). These two samples are from near the basement at Site 597, and they represent the oldest samples analyzed ($\approx$25 to 28 Ma). Sample 2 contains phillipsite, which was not detected in Sample 3. However, phillipsite is probably not a factor in producing the shift to the right, because Samples 1 and 4 (Fig. 4) also contain phillipsite. One possibility is that these two samples contain a terrigenous clastic component of suitable composition to raise preferentially the $^{206}Pb/^{204}Pb$ values. However, Dasch (1981) found that $^{207}Pb/^{204}Pb$ and $^{208}Pb/^{204}Pb$ correlated more closely with the clastic component than did $^{206}Pb/^{204}Pb$ for sediments of the Nazca Plate to the east of the EPR; hence, this explanation does not appear likely.

The Pb isotope compositions of the samples that were treated with a second acid leach are almost identical to the compositions following the first leach. In fact, for four of the six leach pairs, the compositions are indistinguishable, given an analytical uncertainty of 0.1% (e.g., samples 7 *(1)* and 7 *(2)* in Table 1A). For the remaining two leach pairs, the Pb is slightly more radiogenic after the second leach in one case, but is slightly less so in the other. We therefore conclude that there is no significant or systematic difference in the Pb isotope composition of the leach pairs. This conclusion suggests that at least on the scale of the sample, the distribution of Pb is isotopically nearly homogeneous throughout the noncarbonate fraction. (On the basis of the Pb isotope analysis of different size fractions of a metalliferous sample from the Nazca Plate, Dasch [1981] concluded that isotopic homogeneity existed on the scale of the sample.)

In Figure 5, the Leg 92 data are compared with Pb isotope results on other eastern Pacific pelagic and metalliferous sediments ranging in age from Miocene to Recent. The Leg 92 array is similar in terms of its range of $^{206}Pb/^{204}Pb$ values to the Nazca Plate array given by Dasch (1981). The Nazca Plate data, which represent surface sediment analyzed on a bulk-sample basis, display slightly higher $^{208}Pb/^{204}Pb$ and $^{207}Pb/^{204}Pb$ values than the Leg 92 array. These values are probably higher because the sediments of the Nazca Plate, which lies between the EPR and the South American continent, are subjected to a greater detrital influence from the east. Dasch (1981) in fact found that both $^{208}Pb/^{204}Pb$ and $^{207}Pb/^{204}Pb$ correlate more closely than $^{206}Pb/^{204}Pb$ with the calculated "detrital" component of the sediment (correlation coef-

ficient $r = 0.89$ for both $^{208}Pb/^{204}Pb$ and $^{207}Pb/^{204}Pb$ but only 0.68 for $^{206}Pb/^{204}Pb$). Furthermore, he found that changes in the former ratios also correlate with increasing distance east of the EPR, that is, with increasing proximity to South America. Hence, it would appear by comparison that the Leg 92 data reflect a very low detrital component in the sediment. The small size of the detrital component has been substantiated by measurements of the insoluble residue after the application of a third leach to remove the remaining nonclastic material: the residues represented <7% of the noncarbonate fraction in all samples except Samples 1 and 12 (where they represented 13 and 34%, respectively). Hence, the Leg 92 samples consist of a mixture of pelagic carbonate sediment and a significant metalliferous component, with a generally very limited detrital component. Given that the concentration of Pb in the metalliferous (noncarbonate nonresidue) fraction of the samples is at least 180 ppm (Table 1B), the Pb associated with detrital phases (generally <30 ppm: Turekian and Wedepohl, 1961; Wedepohl, 1974) is unlikely to have a significant effect on the overall Pb isotope composition of the sediments analyzed (noncarbonate, but residue bearing).

It should be noted that a few of Dasch's (1981) samples, plotted in the lower diagram of Figure 5, do not come from the Nazca Plate, but from locations slightly west of the EPR, on the eastern margin of the Pacific Plate. These samples are located within 2° of latitude and 3° of longitude of Leg 92 Sites 600 to 602. Their Pb isotope values, which are the least radiogenic in Dasch's entire data set (except for one sample), fall within the least radiogenic portion of the Leg 92 array. This range of values is consistent with the ridge-proximal location of Dasch's samples, which are from within 150 km of the EPR axis.

Sr Isotopes

Sr isotope compositions and Sr concentrations for the sediment samples are given in Tables 1A and 1B. Sr isotope ratios of the noncarbonate fraction show a significant range of values (from 0.7082 to 0.7091, if Sample 5 is excluded as anomalous). The lower ratios are well outside the value of 0.70910 ± 6 for modern-day seawater (Veizer and Compston, 1974). There are a number of explanations for the lower values, the most likely being perhaps change in the Sr isotope composition of seawater with time. As Veizer and Compston (1974) and Burke et al. (1982) have shown from the study of marine carbonates, there has been a gradual change in the Sr isotope composition of seawater during the Phanerozoic to progressively higher $^{87}Sr/^{86}Sr$ ratios in younger sedimentary carbonates. Examination of the data in Table 1A for samples subjected only to the carbonate-removing leach indicates the following:

1. At Site 597, the two samples (2 and 3) with a restricted age bracket (24.8 to 28.3 Ma) have ratios of 0.70826 ± 2.

2. At Site 598, a 1.9-to-5.4-Ma sample (4) and a 14.2-to-17.0-Ma sample (6) have ratios of 0.70892 ± 1 (Sample 5 is anomalous).

3. At Site 599, six samples in the 3.7-to-8.2-Ma age bracket have ratios of 0.709000 ± 2.

4. At Sites 600 to 601, two samples in the 3.7-to-4.6-Ma age bracket have ratios of 0.70906 ± 2.

The preceding data, with the exception of the data for Samples 4 and 5 (both of which are from Site 598), are in extremely close agreement with the seawater Sr isotope composition versus age curve of Burke et al. (1982). The simplest explanation for the agreement is that seawater Sr is released from biogenic carbonate in the sediment during recrystallization and incorporated into the ferromanganiferous phases (older biogenic carbonate initially would have had lower Sr isotopic ratios). Unpublished data indicate that the carbonate phase (removed by the first leach) typically contains about 1000 ppm Sr. Hence, release of some of this Sr could control the Sr isotope composition of the ferromanganiferous phases, particularly since carbonate is the dominant component of most of the sediments (the ratio of the carbonate to the ferromanganiferous phases ranges from 3:1 to 9:1).

Another possible explanation for the lower Sr isotope ratios is a simple linear mixing model like that suggested for Pb; the end-members would be seawater Sr and basaltic Sr derived from the underlying igneous basement. Fresh MORBs have an average $^{87}Sr/^{86}Sr$ value of 0.7027 (Hart, 1976), and hydrothermal solutions that have leached Sr from the basaltic crust should have isotope values close to this figure. That they in fact do has been shown by the discovery of "black smoker" sulfide chimneys on the EPR (RISE Project Group, 1980). These smokers, which are discharging 350°C solutions directly into seawater, have $^{87}Sr/^{86}Sr$ ratios of 0.7031 (Albarede et al., 1981; von Damm et al., 1983). If this value is taken as an end-member value for undiluted hydrothermal solutions, and 0.7091 is taken as the seawater value, the component of basaltic Sr in the sediments from Sites 598 to 601 (although not those from Site 597, as discussed below) can be calculated as being no more than 3% (corresponding to an $^{87}Sr/^{86}Sr$ ratio of 0.7089). Dasch et al. (1971) reported a value of 0.7088 for the noncarbonate fraction of a metalliferous near-surface sample from the Bauer Basin, and concluded that no more than 3% basaltic Sr was present, the remaining Sr being of seawater origin. In the case of the Galapagos hydrothermal mounds, a Mn crust, one nontronite sample, and a sample of normal pelagic nannofossil-rich ooze, gave identical seawater $^{87}Sr/^{86}Sr$ values of 0.7091 (Barrett and Friedrichsen, 1982). However, a second nontronite sample had a value of 0.7089 and was considered to contain about 3% basaltic Sr.

In this interpretation involving basaltic Sr, the Sr is assumed to be in dissolved form initially, but is eventually incorporated into the sediment by some precipitation/absorption mechanism. However, the presence of a few percent of fine-grained volcaniclastic material in the sediment could also have the effect of lowering the Sr isotope ratios of the total carbonate-free fraction. This is because typical (unaltered) MORB contains about 120 ppm Sr (Hart, 1976; Yamaguchi et al., 1977). Unpublished data for our Leg 92 samples indicate that the in-

soluble residue following a third acid leach is generally less than 7% of the noncarbonate fraction. Assuming a 7% volcaniclastic component, approximately 8 ppm basaltic Sr would be contributed to the sediment. Since the noncarbonate fraction typically contains in excess of 300 ppm Sr (Table 1B and unpublished data), the basaltic Sr contributed by a volcaniclastic component could reach some 2.5%. This would be almost sufficient to account for the lowering of the Sr isotope ratios at Sites 598 to 601, although not at Site 597, where some other mechanism or mechanisms are required.

A final possible explanation for the lowering of the Sr isotope ratios of the overall carbonate-free fraction invokes low temperature alteration of the basement well away from the ridge axis. Seawater circulation through the basaltic crust can continue for some millions of years after the formation of the crust, and is known to lead to an increase in the $^{87}Sr/^{86}Sr$ ratio of the basalts through isotope exchange processes (cf. Staudigel et al., 1981). It follows that some basaltic Sr will be liberated during the exchange, which could lead to a decrease in the $^{87}Sr/^{86}Sr$ ratio of the circulating seawater. (The extent of this decrease would depend largely on the overall water/rock ratio during the period of interaction.) If the modified Sr in the crustal waters then diffuses upward through the sediment column and becomes incorporated into recrystallizing mineral phases, lowering of the overall $^{87}Sr/^{86}Sr$ ratio of the (noncarbonate) sediment conceivably could result. This effect would be difficult to distinguish from an earlier, purely hydrothermal contribution of basaltic Sr at the ridge axis. Such a process could have operated at length at Site 597, where all of the sediments below the uppermost 1.5 m are older than ≈14 Ma, and where Sr isotopic ratios are as low as 0.7082. To reiterate, however, the simplest explanation for most of the data from all of the sites (including 597) requires neither hydrothermal or volcaniclastic basaltic Sr, but only the liberation of biogenic Sr from the abundant carbonate phase during recrystallization, and the subsequent incorporation of such Sr into the ferromanganiferous phases.

Table 1A indicates that the Sr isotopic composition of samples treated with a second leach is slightly to distinctly lower than values for the overall carbonate-free fraction. But, this must be considered in the light of the much different Sr concentrations in these leach pairs. Sr concentration data for five samples (Table 1B) indicate that the carbonate-free fraction of the sediment typically contains 370 to 430 ppm Sr. As in the case of Pb, this value is the sum of the Sr removed in the two leach treatments (second and third) *following removal of the carbonate fraction*, and excludes any Sr associated with detrital silicate phases. Of this 370 to 430 ppm Sr, only 12 to 42 ppm are in the third leach. As discussed earlier, insoluble volcaniclastic phases possibly present in minor amounts in the isotopically analyzed samples could contribute perhaps 10 ppm basaltic Sr to the samples. Hence, the residue following the second leach could contain a mixture of seawater and basaltic Sr, and therefore display notably lowered Sr isotopic ratios. By contrast, the overall carbonate-free fraction (i.e., residue after the first leach) would display Sr isotopic ratios only slightly lower than seawater values if the ≈350 to 400 ppm Sr present in the *soluble* phases is all of seawater derivation.

It should be noted that the reason that the Leg 92 metalliferous sediments contain a distinct basaltic Pb component, but a primarily seawater-derived Sr concentration, is related to the relative abundance of these elements in seawater and basalt. Although basalts contain two orders of magnitude more Sr than Pb (≈120 ppm vs. ≈1 ppm; Church and Tatsumoto, 1975; Hart, 1976; Unruh and Tatsumoto, 1976; Yamaguchi et al., 1977), seawater contains six orders of magnitude more Sr than Pb (≈8 ppm vs. 2×10^{-6} to 3×10^{-5} ppm; Goldberg, 1965; Veizer and Compston, 1974; C.C. Patterson, in Tatsumoto, 1978). A given volume of discharging solution which had leached (or isotopically exchanged with) 1% of the Sr and Pb from an equal volume of basement would contain ≈1 ppm basaltic Sr and ≈0.01 ppm basaltic Pb. Mixture with an equal volume of normal seawater (or even 10 volumes of seawater) would still produce a solution dominated by seawater Sr and basaltic Pb.

Rare Earth Elements

The rare earth element distribution patterns of recent metalliferous sediments are broadly similar to those of deep-ocean seawater (Bender et al., 1971; Dymond et al., 1974; Piper and Graef, 1974; Toth, 1980; Marchig et al., 1982; Fleet, 1983). The patterns show comparatively little variation despite strong fractionation of the REE (particularly Ce and Eu) at various depths in the water column (Elderfield and Greaves, 1982). Shale-normalized patterns of recent metalliferous sediments at the EPR are characterized by a marked depletion in Ce relative to its neighbors La and Pr, and a modest enrichment in the heavy (HREE) relative to the light (LREE) rare earth elements. The Ce anomaly, Ce*, may be defined as follows:

$$Ce^* = \log \{Ce_{sh}/[0.5 \times (La_{sh} + Pr_{sh})]\}$$

where Ce_{sh}, La_{sh}, and Pr_{sh} are the shale-normalized values of each element.

Rare earth element patterns for selected samples from Sites 597 to 601 are shown in Figure 6; concentrations are given in ppm in Table 2. The Leg 92 sediments have similar total REE contents, which range on a carbonate-free basis from 131 to 301 ppm, with a clustering between 167 and 222 ppm (except for two surficial samples, which will be discussed later). The patterns have strong negative Ce anomalies (Ce* ranges from −0.56 to −0.90, with a clustering between −0.72 and −0.87). The samples from Sites 599 and 601 have almost identical patterns which display a slight but consistent enrichment in the HREE relative to the LREE, whereas the samples from Sites 597 and 598 have flatter HREE patterns. By contrast, the metalliferous sediments from the crest of the EPR show a distinct enrichment in HREE over the LREE (Piper and Graef, 1974; Marchig et al., 1982). The Leg 92 sediment patterns also differ markedly from those of the pelagic clays (montmorillonitic)

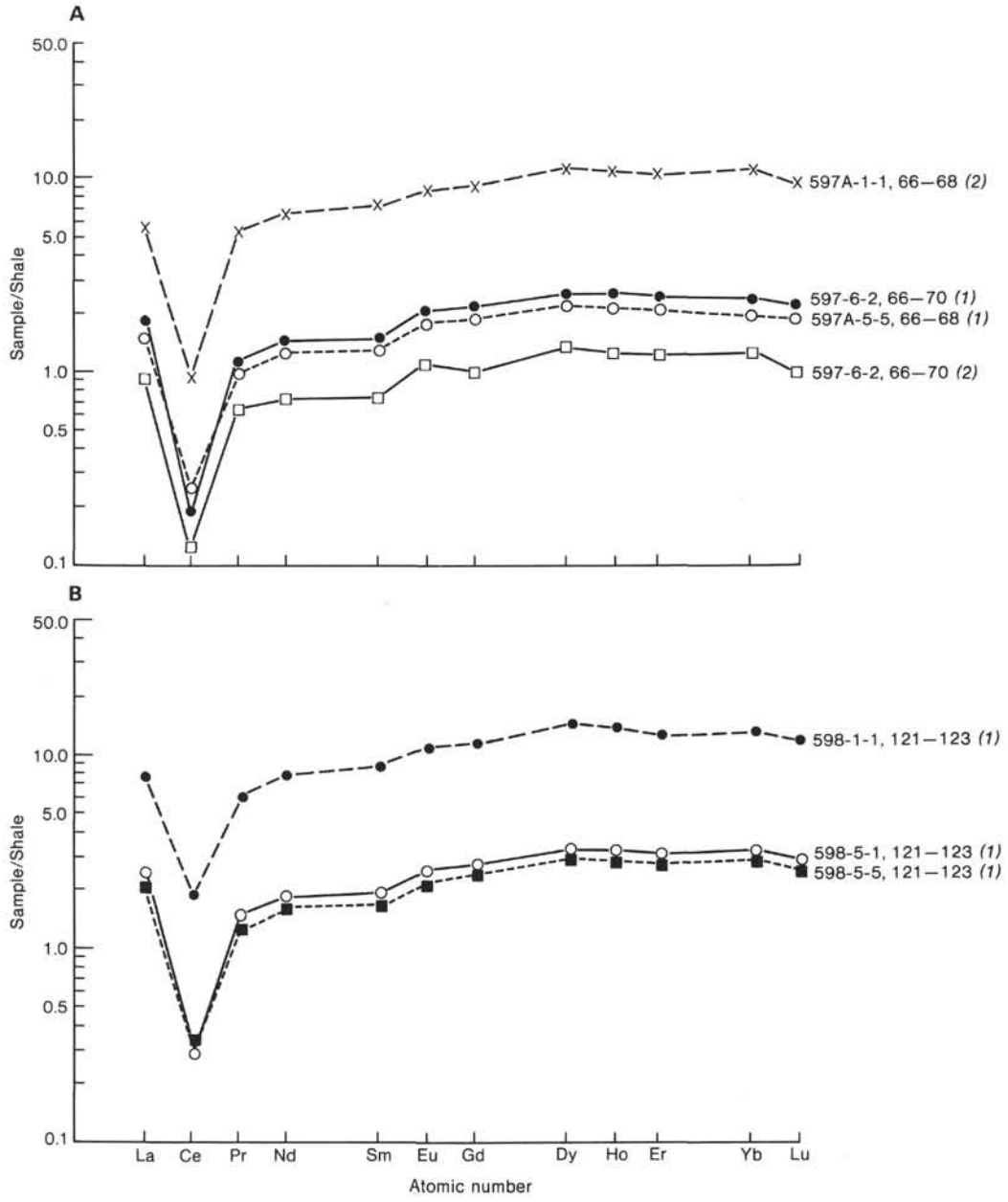

Figure 6. REE patterns for samples from DSDP Leg 92. REE values are normalized to average shale (Haskin and Haskin, 1966; Piper, 1974a). Concentrations are given in ppm in Table 2. *(1)* and *(2)* as defined for Figure 3. A. Site 597. B. Site 598. C. Site 599. (The REE patterns for Samples 599B-2-6, 121–123 *(1)* and 599-4-5, 121–123 *(1)* lie between the upper dashed line and the solid line.) D. Sites 600 to 601 and the Leg 92 sediment standard.

from the northern Pacific, which have flat patterns with no Ce anomaly (Piper, 1974a, b; Elderfield et al., 1981).

Geochemical and mineralogical considerations suggest that the REE in metalliferous sediments like those at the EPR were originally sequestered from seawater. A direct hydrothermal source is unlikely, because REE distributions in hydrothermal solutions from the EPR are characterized by a large positive Eu anomalies (Michard et al., 1983) and are strongly depleted in the HREE relative to the LREE. Metalliferous sediments with patterns of this latter type are in fact known from the Red Sea (Courtois and Treuil, 1977). The seawater pattern of sediments like those at the EPR appears to result from the rapid precipitation and adsorption of seawater REEs (without fractionation) onto hydrothermally derived Fe–Mn oxyhydroxide colloidal particles in the water column or shortly after the particles have settled onto the seafloor. A primary seawater source for Nd and Sr in metalliferous sediments from the eastern Pacific is also indicated by their $^{143}Nd/^{144}Nd$ and $^{87}Sr/^{86}Sr$ ratios, which are very close to seawater values (O'Nions et al., 1978; Piepgras et al., 1979; Elderfield et al., 1981; Goldstein and O'Nions, 1981).

As noted above, samples from Sites 599 to 601 display a slight enrichment in the HREEs. Since the deposits at the EPR are enriched in the HREE, we inter-

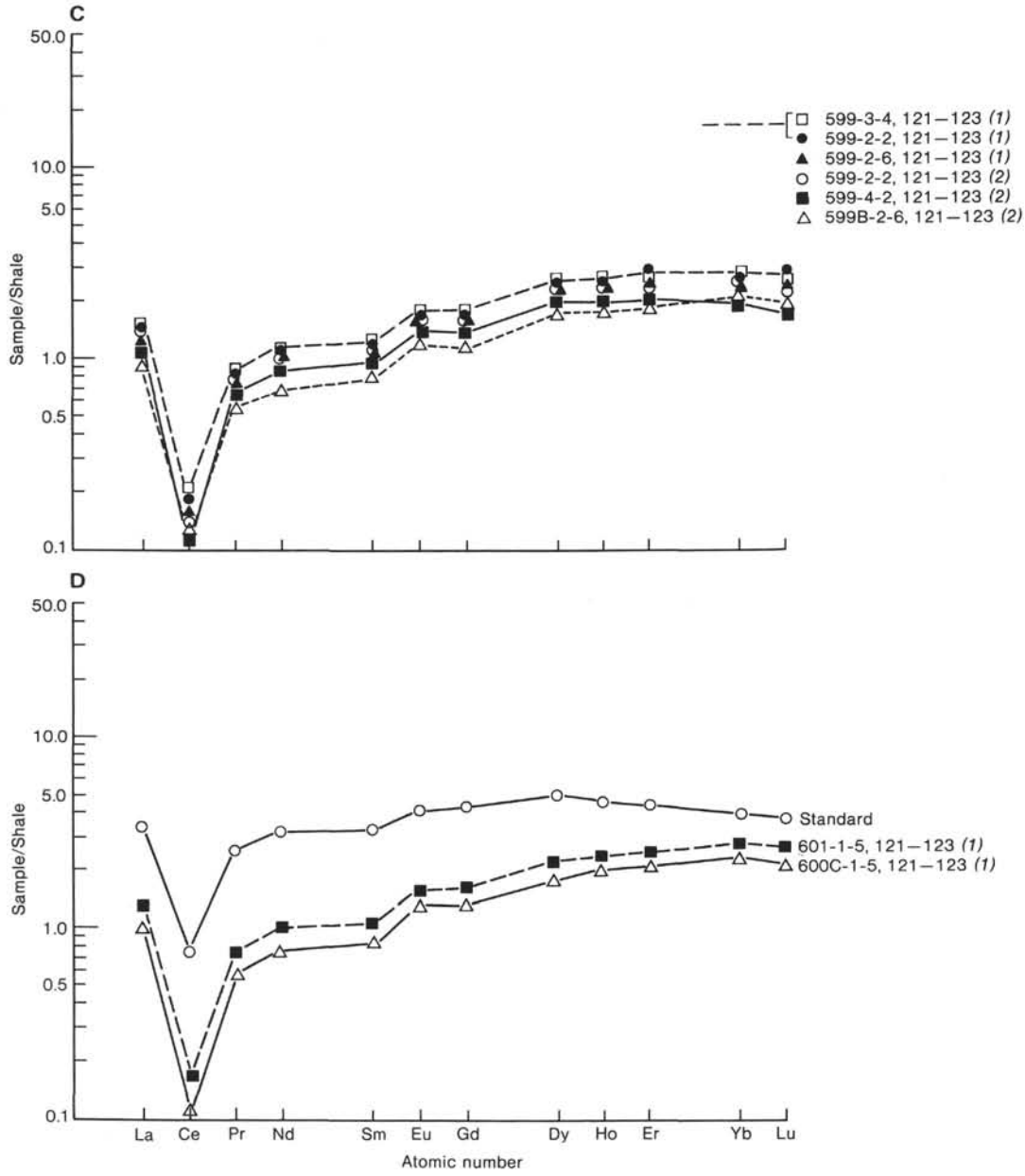

Figure 6 (continued).

pret the data from these sites as reflecting the presence of an original EPR component which has been somewhat modified during diagenesis. We then infer from the flattened HREE patterns of Sites 597 and 598 that further diagenetic modification has removed the remaining HREE enrichment. One such mechanism might be recrystallization of the original Fe-bearing and P-bearing phases in the sediment, as discussed below.

The diagenetic history of metalliferous sediments formed at the EPR can be expected to alter the initial REE patterns. At least some of the original Fe-oxyhydroxide phases in surficial EPR crestal sediments commonly undergoes a transition to Fe-smectite as a result of reaction with biogenic opal during diagenesis. Because the large ionic radii of the REEs preclude their substitution in either the tetrahedral or octahedral lattice sites of the smectite structure, some are released into solution or lost to other phases during the formation of the Fe-smectite. In contrast, biogenic apatite originally present in the sediment acquires REE during diagenesis (Dymond and Eklund, 1978). Elderfield et al. (1981) have found that the concentrations of REE (excluding Ce) in northern equatorial Pacific sediments are correlated closely with P content, and infer that they are associated with phosphatic dish debris. They also found that the P-rich phase was slightly depleted in the HREE (relative to a flat pattern). These authors suggest that where the diagenetic smectite-forming reaction is involved, some of the REEs originally associated with Fe-oxyhydroxides undergo a type of intra-sediment transferral to the phosphatic phase. Another probable example of the action of this process is the Leg 85 metalliferous sediment, which formed under the equatorial belt of opal production some 2000 km north of the Leg 92 sediments (Jarvis, 1985). In the

Table 2. Rare earth element composition (in ppm) of noncarbonate fraction of selected samples from DSDP Leg 92 (shale-normalized values in parentheses).

Sample no. in Table 1[a] DSDP Sample no.	1 *(2)* 597A-1-1 (66–68)	2 *(1)* 597A-5-5 (66–68)	3 *(1)* 597-6-2 (66–70)	3 *(2)* 597-6-2 (66–70)	4 *(1)* 598-1-1 (121–123)	5 *(1)* 598-5-1 (121–123)	6 *(1)* 598-5-5 (121–123)	7 *(1)* 599-2-2 (121–123)	7 *(2)* 599-2-2 (121–123)
Y	481	97.2	114	50.8	615	136	126	119	110
La	250 (6.09)	64.0 (1.56)	77.0 (1.88)	39.1 (0.95)	305 (7.43)	107 (2.61)	88.3 (2.15)	61.5 (1.50)	57.2 (1.4)
Ce	78.7 (0.95)	19.6 (0.24)	15.7 (0.19)	9.78 (0.12)	152 (1.83)	24.8 (0.30)	27.7 (0.33)	14.8 (0.18)	11.2 (0.14)
Pr	54.5 (5.39)	10.2 (1.01)	11.2 (1.11)	6.43 (0.64)	60.4 (5.98)	15.3 (1.52)	13.4 (1.32)	8.56 (0.85)	8.48 (0.84)
Nd	247 (6.49)	49.6 (1.30)	54.8 (1.44)	27.3 (0.72)	295 (7.76)	72.2 (1.90)	64.0 (1.68)	42.5 (1.12)	39.3 (1.03)
Sm	54.0 (7.07)	10.0 (1.34)	10.8 (1.44)	5.55 (0.74)	61.8 (8.24)	14.3 (1.91)	13.2 (1.76)	8.80 (1.17)	8.39 (1.12)
Eu	14.2 (8.85)	2.99 (1.88)	3.33 (2.07)	1.75 (1.09)	16.4 (10.2)	4.12 (2.56)	3.75 (2.33)	2.84 (1.76)	2.72 (1.69)
Gd	59.0 (9.29)	12.0 (1.89)	13.3 (2.09)	6.28 (0.99)	72.2 (11.4)	17.0 (2.86)	15.8 (2.49)	10.9 (1.72)	10.2 (1.60)
Dy	65.9 (11.9)	12.6 (2.29)	13.8 (2.51)	7.47 (1.36)	75.8 (13.8)	17.8 (3.24)	16.7 (3.02)	13.5 (2.45)	12.6 (2.30)
Ho	14.6 (10.9)	2.92 (2.18)	3.37 (2.51)	1.63 (1.22)	17.0 (13.3)	4.22 (3.14)	3.95 (2.95)	3.27 (2.43)	3.08 (2.29)
Er	38.5 (10.3)	7.96 (2.12)	8.87 (2.36)	4.48 (1.20)	47.2 (12.6)	11 5 (3.05)	10.5 (2.80)	11.1 (2.95)	8.62 (2.30)
Yb	38.9 (11.0)	6.91 (1.96)	8.30 (2.36)	4.35 (1.23)	44.8 (12.7)	11.1 (3.13)	10.3 (2.91)	9.26 (2.64)	9.00 (2.55)
Lu	5.97 (9.30)	1.11 (1.83)	1.30 (2.13)	0.59 (0.97)	7.02 (11.5)	1.66 (2.72)	1.60 (2.63)	1.58 (2.59)	1.35 (2.21)
ΣREE[b]	910	200	222	115	1155	301	269	189	172
Ce*[c]	−0.78	−0.73	−0.90	−0.82	−0.56	−0.84	−0.72	−0.81	

Note: All data given on a salt-free basis.
[a] *(1)* and *(2)* as defined in Table 1A.
[b] ΣREE is the sum of the measured REE concentrations (excluding Y).
[c] Ce* is the magnitude of the (negative) Ce anomaly and is defined in the text.

case of the Leg 85 sediments, Jarvis found a good correlation between REE and P contents, and an additional poorer one between REE and Fe contents. Since the sediments he examined also contained a goethitic phase, the REE associated with this phase may have been responsible for the secondary correlation (the more abundant Fe-smectite in these sediments would tend to reject the REEs). If so, the resulting REE pattern for the bulk sediment would be the sum of the contributions of the goethitic and apatitic phases (any biogenic carbonate present would have an insignificant effect on the patterns as a result of the very low REE contents of this phase; Elderfield et al., 1981).

In the case of the Leg 92 samples, Fe-smectite can only be a minor phase. None was detected by XRD, and unpublished data on Si content indicate that Fe-smectite cannot exceed about 2% of the noncarbonate fraction. The Leg 92 patterns therefore must reflect the apatitic and goethitic components of the sediment. The apatitic component of the samples analyzed by Elderfield et al. (1981) is slightly HREE depleted. At present, there is no information for the region of Leg 92 on the REE patterns of any purely goethitic phases formed during sediment diagenesis. However, ferromanganese nodules that have grown under diagenetic influence in the area consist of discrete apatitic and Fe-oxyhydroxide phases, the former slightly depleted in the HREE (relative to a flat pattern), and the latter notably depleted in the HREE (Elderfield et al., 1981 and studies cited therein). Although these results from nodules may not be directly applicable to sediments, it seems at least possible that Fe-oxyhydroxide phases in diagenetically altered sediments may also show HREE depletion. If so, then the final REE patterns resulting from advanced diagenesis, regardless of the proportions of smectite, goethite, and apatite formed in the sediment, should show flat patterns or some degree of HREE depletion. A possible explanation for a preferential loss of HREE from sediment phases during diagenesis, if such a loss does in fact occur, is that the dissolved complexes of HREE are more stable than those of LREE (Turner and Whitfield, 1979).

The REE pattern of any Leg 92 (or Leg 85) sediment would depend on the extent to which the original Fe-phase, bearing the EPR signature (HREE enrichment), was still present in the sediment. The degree of HREE enrichment would then depend on the degree of diagenesis, which, all other factors being the same, will depend upon the age of the sediment. As shown in Table 1A, four of the six samples from Sites 597 and 598 are about twice as old as the samples from Sites 599 to 601 (or more). Hence, for these older samples, we suggest that the longer diagenetic history has led to a nearly complete loss of the original EPR HREE enrichment, with a resulting flattened pattern for the HREE.

The other two samples from Sites 597 and 598 (Samples 1 and 4), respectively located $\approx$750 and $\approx$1250 km west of the EPR, are both from within 1.3 m of the surface of the ocean floor. These two samples can be considered apart from the others in that they are characterized by anomalously high REE contents (Table 2), slow accumulation rates, and atypical mineralogies. Both samples have REE contents on the order of 1000 ppm, a factor of 4 to 6 greater than the other sediments analyzed, and both contain significant proportions of phillipsite, which was not detected in the other, deeper sediments. Because these sediments accumulated at significantly slower rates than the other samples analyzed (see site chapters, this volume), diagenetic effects have probably been considerable. Both surficial samples have REE patterns that are similar to Bauer Basin patterns from $\approx$750 km east of the EPR (i.e., they lack an EPR component). It is of interest that in both of these areas, there is evidence for some hydrothermal input into the sediments, as indicated by the Pb isotope values of the two samples (this study), and by the negative Ce anomalies of ferromanganese *nodules* from the Bauer Basin (Elderfield and Greaves, 1981). Hence, it may be that in sediments that are accumulating at very slow rates, diagenetic effects

Table 2 (continued).

8 *(1)* 599-2-6 (121–123)	9 *(1)* 599-3-4 (121–123)	10 *(2)* 599-4-2 (121–123)	11 *(1)* 599-4-5 (121–123)	12 *(1)* 599B-2-6 (121–123)	12 *(2)* 599B-2-6 (121–123)	13 *(1)* 600C-1-5 (121–123)	14 *(1)* 601-2-5 (121–123)	Leg 92 sediment standard	
								Bulk sediment	Carbonate-free fraction
107	124	87.9	118	130	94.3	95.5	118	30.3	186
52.8 (1.29)	63.1 (1.54)	45.2 (1.10)	63.0 (1.54)	50.8 (1.24)	38.2 (0.93)	42.2 (1.03)	54.9 (1.34)	23.4	144 (3.52)
12.9 (0.16)	17.0 (0.21)	9.02 (0.11)	13.2 (0.16)	13.8 (0.17)	9.70 (0.12)	9.65 (0.11)	13.6 (0.16)	10.4	64.0 (0.77)
7.72 (0.76)	8.88 (0.88)	6.99 (0.69)	8.27 (0.82)	7.20 (0.71)	5.81 (0.57)	5.79 (0.57)	7.47 (0.74)	4.34	26.7 (2.65)
38.6 (1.02)	44.4 (1.17)	32.9 (0.86)	41.0 (1.08)	35.8 (0.94)	26.5 (0.69)	29.1 (0.77)	27.4 (0.99)	20.3	125 (3.29)
8.09 (1.08)	9.29 (1.24)	6.98 (0.93)	8.54 (1.14)	8.14 (1.09)	6.00 (0.80)	6.11 (0.82)	7.90 (1.06)	3.97	24.4 (3.25)
2.59 (1.61)	2.91 (1.81)	2.26 (1.40)	2.72 (1.69)	2.58 (1.61)	1.96 (1.22)	2.06 (1.28)	2.52 (1.57)	1.05	6.63 (4.12)
10.2 (1.60)	11.8 (1.85)	8.52 (1.34)	10.9 (1.72)	10.2 (1.61)	7.29 (1.15)	7.87 (1.24)	10.2 (1.60)	4.45	27.4 (4.31)
12.4 (2.25)	13.7 (2.49)	10.6 (1.92)	12.8 (2.33)	13.6 (2.46)	9.59 (1.74)	9.66 (1.76)	12.0 (2.19)	4.45	27.4 (4.98)
3.06 (2.28)	3.52 (2.63)	2.54 (1.89)	3.33 (2.48)	3.22 (2.43)	3.36 (1.76)	2.50 (1.86)	2.95 (2.36)	1.00	6.13 (4.57)
8.98 (2.40)	9.65 (2.57)	7.17 (1.90)	9.16 (2.46)	11.1 (2.96)	6.91 (1.84)	7.16 (1.91)	8.99 (2.57)	2.67	16.4 (4.45)
8.61 (2.44)	9.85 (2.79)	7.43 (2.10)	9.56 (2.71)	9.73 (2.76)	7.65 (2.17)	7.37 (2.08)	9.26 (2.57)	2.26	13.9 (3.96)
1.45 (2.38)	1.56 (2.56)	1.10 (1.80)	1.52 (2.50)	1.81 (2.97)	1.13 (1.86)	1.14 (1.87)	1.51 (2.58)	0.33	2.04 (3.35)
167	196	141	184	168	124	169	131	78.7	484
−0.81	−0.76	−0.91	−0.87	−0.76	−0.80	−0.81	−0.86		

are such that no HREE enrichment is recorded in the REE pattern. The negative Ce anomaly is maintained in the altered sediment, as is the component of hydrothermal Pb, but the heavier REEs appear to be too readily mobilized and lost to solution. An important step in aiding the interpretation of REE patterns of oceanic metalliferous sediments would be a detailed assessment of the degree to which the separate Fe–oxyhydroxide and P-rich phases lose or gain REEs (in particular the HREEs) during progressive diagenetic recrystallization.

ACKNOWLEDGMENTS

T. J. B. gratefully acknowledges research support provided by grants from the Natural Sciences and Engineering Research Council of Canada, and from the University of Toronto. The isotope geology work at Oxford was funded by a research grant from the Natural Environment Research Council to Dr. S. Moorbath, to whom we express our thanks for the use of facilities. Mr. Roy Goodwin provided skilled technical assistance with the isotope analyses. We also express our gratitude to Dr. N. Walsh for providing use of the Inductively Coupled Plasma (ICP) Spectrometer at King's College, London. Additional analytical facilities were kindly provided by the Department of Geology, City of London Polytechnic, and the Institute of Oceanographic Sciences, Wormley (U.K.). We thank Dr. M. Palmer for reviewing this paper and making a number of suggestions which were beneficial to the manuscript.

REFERENCES

Albarede, F., Michaud, A., Minster, J. F., and Michaud, G., 1981. $^{87}Sr/^{86}Sr$ ratios in hydrothermal waters and deposits from the East Pacific Rise at 21°N. *Earth Planet. Sci. Lett.*, 55:229–236.

Am. Assoc. Pet. Geol., 1982. Plate-tectonic map of the circum-Pacific region (Pacific Basin sheet). *Circum-Pacific Map Project, Circum-Pacific Council For Energy and Mineral Resources.* (Publ. by Am. Assoc. Pet. Geol.)

Aoki, S., Kohyama, N., and Sudo, T., 1974. An iron-rich montmorillonite in a sediment core from the northeastern Pacific. *Deep Sea Res.*, 21:865–875.

Barrett, T. J., and Friedrichsen, H., 1982. Elemental and isotopic compositions of some metalliferous and pelagic sediments from the Galapagos Mounds area, DSDP Leg 70. *Chem. Geol.*, 36:275–298.

Bender, M. L., Broecker, W., Gornitz, V., Middel, U., Kay, R., Sun, S. S., and Biscaye, P., 1971. Geochemistry of three cores from the East Pacific Rise. *Earth Planet. Sci. Lett.*, 12:425–433.

Bonatti, E., 1975. Metallogenesis at oceanic spreading centers. *Annu. Rev. Earth Planet. Sci.*, 3:401–431.

Bonatti, E., Kraemer, T., and Tydell, H., 1972. Classification and genesis of submarine iron-manganese deposits. *In* Horn, D. R. (Ed.), *Ferromanganese Deposits on the Ocean Floor*: Washington (NSF), 149–166.

Boström, K., and Peterson, M. N. A., 1966. Precipitates from hydrothermal exhalations on the East Pacific Rise. *Econ. Geol.*, 61:1258–1265.

Boström, K., Peterson, M. N. A., Joensuu, O., and Fisher, D. E., 1969. Aluminum-poor ferromanganese sediments on active ocean ridges. *J. Geophys. Res.*, 74:3261–3270.

Brevart, O., Dupré, B., and Allègre, C. J., 1981. Metallogenesis at spreading centers: lead isotope systematics for sulfides, manganese-rich crusts, basalts, and sediments from the CYAMEX and ALVIN areas (East Pacific Rise). *Econ. Geol.*, 1205–1210.

Burke, W. A., Denison, R. E., Hetherington, E. A., Koepnick, R. B., Nelson, H. F., and Otto, J. B., 1982. Variation of seawater $^{87}Sr/^{86}Sr$ throughout Phanerozoic time. *Geology*, 10:516–519.

Church, S. E., and Tatsumoto, M., 1975. Lead isotope relations in oceanic ridge basalts from the Juan de Fuca–Gorda Ridge area, N. E. Pacific Ocean. *Contrib. Mineral. Petrol.*, 53:253–279.

Corliss, J. B., 1971. The origin of metal-bearing hydrothermal solutions. *J. Geophys. Res.*, 76:8128–8138.

Corliss, J. B., Lyle, M., Dymond, J., and Crane, K., 1978. The chemistry of hydrothermal mounds near the Galapagos Rift. *Earth Planet. Sci. Lett.*, 40:12–24.

Courtois, C., and Treuil, M., 1977. Distribution des terres rares et de quelques éléments en trace dans les sédiments récents des fosses de la Mer Rouge. *Chem. Geol.*, 20:57–72.

Cronan, D. S., 1973. Basal ferruginous sediments cored during Leg 16, Deep Sea Drilling Project. *In* van Andel, T. H., Heath, G. R., et al., *Init. Repts. DSDP*, 16: Washington (U.S. Govt. Printing Office), 601–604.

_____, 1976. Basal metalliferous sediments from the eastern Pacific. *Geol. Soc. Am. Bull.*, 87:928–934.

_____, 1980. *Underwater Minerals*: London (Academic Press).

Cronan, D. S., and Garrett, D. A., 1973. Distribution of elements in metalliferous Pacific sediments collected during the Deep Sea Drilling Project. *Nature London Phys. Sci.*, 242:88–89.

Dasch, E. J., 1981. Lead isotopic composition of metalliferous sediments from the Nazca Plate. *Mem. Geol. Soc. Am.*, 154:199–209.

Dasch, E. J., Dymond, J. R., and Heath, G. R., 1971. Isotopic analysis of metalliferous sediments from the East Pacific Rise. *Earth Planet. Sci. Lett.*, 13:175–180.

Dymond, J., 1981. Geochemistry of Nazca plate surface sediments: an evaluation of hydrothermal, biogenic, detrital, and hydrogenous sources. *Mem. Geol. Soc. Am.*, 154:133–173.

Dymond, J., Corliss, J. B., Heath, G. R., Field, C. W., Dasch, E. J., and Veeh, H. H., 1973. Origin of metalliferous sediments from the Pacific Ocean. *Geol. Soc. Am. Bull.*, 84:3355–3372.

Dymond, J., Corliss, J. B., and Stillinger, R., 1976. Chemical composition and metal accumulation rates of metalliferous sediments from Sites 319, 320 and 321. *In* Yeats, R. S., Hart, S. R., et al., *Init. Repts. DSDP*, 34: Washington (U.S. Govt. Printing Office), 575–588.

Dymond, J., and Eklund, W., 1978. A microprobe study of metalliferous sediment components. *Earth Planet. Sci. Lett.*, 40:243–251.

Dymond, J., and Veeh, H. H., 1975. Metal accumulation rates in the southeast Pacific and the origin of metalliferous sediments. *Earth Planet. Sci. Lett.*, 28:13–22.

Elderfield, H., and Greaves, M. J., 1981. Negative cerium anomalies in the rare-earth element patterns of oceanic ferromanganese nodules. *Earth Planet. Sci. Lett.*, 55:163–170.

_____, 1982. The rare-earth elements in seawater. *Nature London*, 296:214–219.

Elderfield, H., Hawkesworth, C. J., Greaves, M. J., and Calvert, S. E., 1981. Rare-earth element geochemistry of oceanic ferromanganese nodules and associated sediments. *Geochim. Cosmochim. Acta*, 45:513–528.

Field, C. W., Wetherell, D. G., and Dasch, E. J., 1981. Economic appraisal of Nazca Plate metalliferous sediments. *Mem. Geol. Soc. Am.*, 154:315–320.

Fleet, A. J., 1983. Hydrothermal and hydrogenous ferro-manganese deposits: do they form a continuum? The rare earth element evidence. *In* Rona, P. A., Boström, K., Laubier, L., and Smith, K. L. (Eds.), *Hydrothermal Processes at Seafloor Spreading Centers:* New York (Plenum), 535–555.

Goldberg, E. D., 1965. The minor constituents of seawater. *In* Riley, J. P., and Skirrow, G. (Eds.), *Chemical Oceanography* (Vol. 2): New York (Academic Press), 163–196.

Goldstein, S. L., and O'Nions R. K., 1981. Nd and Sr isotopic relationships in pelagic clays and ferromanganese deposits. *Nature London*, 292:324–327.

Hart, S. R., 1976. LIL-element geochemistry, Leg 34 basalts. *In* Yeats, R. S., Hart, S. R., et al., *Init. Repts. DSDP*, 34: Washington (U.S. Govt. Printing Office), 283–288.

Haskin, M. A., and Haskin, L. A., 1966. Rare earths in European shales: a redetermination. *Science Washington D.C.*, 154:507–509.

Hays, J. D., et al., 1972. *Init. Repts. DSDP*, 9: Washington (U.S. Govt. Printing Office).

Heath, G. R., and Dymond, J., 1977. Genesis and transformation of metalliferous sediments from the East Pacific Rise, Bauer Deep, and Central Basin, northwest Nazca Plate. *Geol. Soc. Am. Bull.*, 88:723–733.

_____, 1981. Metalliferous-sediment deposition in time and space: East Pacific Rise and Bauer Basin, northern Nazca Plate. *Mem. Geol. Soc. Am.*, 154:175–197.

Hein, J. R., Yeh, H.-W., and Alexander, E., 1979. Origin of iron-rich montmorillonite from the manganese nodule belt of the north equatorial Pacific. *Clays Clay Mineral.*, 27:185–194.

Hekinian, R., Rosendahl, B. R., Cornan, D. S., Dmitriev, Y., Fodor, R. V., Goll, R. M., Hoffert, M., Humphris, S. E., Mattley, D. P., Natland, J., Peterson, W., Roggenthen, W., Schrader, E., Scrivastava, R. K., and Warren, N., 1978. Hydrothermal deposits and associated basement rocks from the Galapagos Spreading Center. *Oceanol. Acta*, 1:473–482.

Honnorez, J., Von Herzen, R. P., et al., 1983. *Init. Repts. DSDP*, 70: Washington (U.S. Govt. Printing Office).

Honnorez, J., Von Herzen R. P., Barrett, T., Becker, K., Borella, P., Hubberten, H. W., Jones, S., Karato, S., Laverne, C., Levi, S., Migdisov, A. A., Moorby, S. A., and Schrader, E., 1981. Hydrothermal mounds and young oceanic crust of the Galapagos: preliminary Deep Sea Drilling results, Leg 70. *Geol. Soc. Am. Bull.*, 92:457–472.

Jarvis, I., 1985. Geochemistry and origin of Eocene–Oligocene metalliferous sediments from the central equatorial Pacific: Deep Sea Drilling Project Sites 573 and 574. *In* Mayer, L., Theyer, F., et al., *Init. Repts. DSDP*, 85: Washington (U.S. Govt. Printing Office), 781–804.

Jarvis, I., and Jarvis, K. E., 1985. Rare-earth element geochemistry of standard sediments: a study utilizing inductively coupled plasma spectrometry. *Chem. Geol.*, 53:335–344.

Leinen, M., 1981. Metal-rich basal sediments from northeastern Pacific Deep Sea Drilling Project sites. *In* Yeats, R. S., Haq, B. U., et al., *Init. Repts. DSDP*, 63: Washington (U.S. Govt. Printing Office), 667–676.

Lyle, M., 1981. Formation and growth of ferromanganese oxides on the Nazca Plate. *Mem. Geol. Soc. Am.*, 154:269–293.

McMurtry, G. M., Veeh, H. H., and Moser, C., 1981. Sediment accumulation rate patterns on the northwest Nazca Plate. *Mem. Geol. Soc. Am.*, 154:211–249.

Marchig, V., and Gundlach, H., 1982. Iron-rich metalliferous sediments on the East Pacific Rise—prototype of undifferentiated metalliferous sediments in divergent plate boundaries. *Earth Planet. Sci. Lett.*, 58:361–382.

Marchig, V., Gundlach, H., Moller, P., and Schley, F., 1982. Some geochemical indicators for discriminating between diagenetic and hydrothermal metalliferous sediments. *Mar. Geol.*, 50:241–256.

Mayer, L., Theyer, F., Barron, J. A., Dunn, D. A., Handyside, T., Hills, S., Jarvis, I., Nigrini, C. A., Pisias, N. G., Pujos, A., Stout, P., Thomas, E., Weinreich, N., and Wilkens, R. H., 1982. *Challenger* returns to Pacific. *Geotimes*, 27:19–20.

Michard, A., Albarede, F., Michard, G., Minster, J. F., and Charlou, J. L., 1983. Rare-earth elements and uranium in high-temperature solutions from East Pacific Rise hydrothermal vent field (13°N). *Nature London*, 303:795–797.

Moorby, S. A., 1983. The geochemistry of transitional sediments recovered from the Galapagos Hydrothermal Mounds Field during DSDP Leg 70—implications for mounds formation. *Earth Planet. Sci. Lett.*, 62:367–376.

Murray, J., and Renard, A. F., 1891. *Deep Sea Deposits: Report of the Scientific Results of the HMS* Challenger, *1873–1876*: London (HMSO).

O'Nions, R. K., Carter, S. R., Cohen, R. S., Evensen, N. M., and Hamilton, P. J., 1978. Pb, Nd, and Sr isotopes in oceanic ferromanganese deposits and ocean floor basalts. *Nature London*, 273: 435–438.

O'Nions, R. K., and Pankhurst, R. J., 1973. Determination of Rb/Sr and $^{37}Sr/^{86}Sr$ ratios of some standard rocks and evaluation of X-ray fluorescence spectrometry in Rb–Sr geochemistry. *Chem. Geol.*, 12:127–1136.

Piepgras, D. J., Wasserberg, G. J., and Dasch, E. J., 1979. The isotopic composition of Nd in different ocean masses. *Earth Planet. Sci. Lett.*, 45:223–236.

Piper, D. Z., 1973. Origin of metalliferous sediments from the East Pacific Rise. *Earth Planet. Sci. Lett.*, 19:75–82.

_____, 1974a. Rare-earth elements in ferromanganese nodules and other marine phases. *Geochim. Cosmochim. Acta*, 38:1007–1022.

_____, 1974b. Rare-earth elements in the sedimentary cycle: a summary. *Chem. Geol.*, 14:285–304.

Piper, D. Z., and Graef, P. A., 1974. Gold and rare-earth elements in sediments from the East Pacific Rise. *Mar. Geol.*, 17:287–297.

Revelle, R., 1944. Marine bottom samples collected in the Pacific Rise Ocean by the Carnegie on its seventh cruise. *Carnegie Inst. Washington Publ.*, 556:1–180.

Reynolds, P. H., and Dasch, E. J., 1971. Lead isotopes in marine Mn nodules and the ore-lead growth curve. *J. Geophys. Res.*, 76:5124–5129.

RISE Project Group, 1980. East Pacific Rise: hot springs and geophysical experiments. *Science Washington D.C.*, 207:1421–1433.

Sayles, F. L., and Bischoff, J. L., 1973. Ferromanganese sediments in the equatorial east Pacific. *Earth Planet Sci. Lett.*, 19:330–336.

Sayles, F. L., Ku, T. L., and Bowker, P. C., 1975. Chemistry of ferromanganese sediment of the Bauer Deep. *Geol. Soc. Am. Bull.*, 86: 1423–1431.

Stacey, J. S., and Kramers, J. D., 1975. Approximation of terrestrial lead isotopes evolution by a two-stage model. *Earth Planet. Sci. Lett.*, 26:207–221.

Staudigel, H., Hart, S. R., and Richardson, S. H., 1981. Alteration of the ocean crust: processes and timing. *Earth Planet. Sci. Lett.*, 52: 311–327.

Sun, S.-S., 1973. Lead isotope studies of young volcanic rocks from oceanic islands, mid-ocean ridges and island areas [Ph.D. dissert.]. Columbia Univ., New York.

Tatsumoto, M., 1978. Isotopic composition of lead in oceanic basalt and its implication to mantle evolution. *Earth Planet. Sci. Lett.*, 38:63–87.

Thompson, G., 1983. Basalt–seawater interaction. *In* Rona, P. A., Boström, K., Laubier, L., and Smith, K. L. (Eds.), *Hydrothermal Processes at Seafloor Spreading Centers:* New York (Plenum), 225–278.

Thompson, M., and Walsh, J. N., 1983. *A Handbook of Inductively Coupled Plasma Spectrometry*: Glasgow (Blackie & Son).

Toth, J. R., 1980. Deposition of submarine hydrothermal iron and evidence for hydrothermal input of volatile elements to the oceans. *Geol. Soc. Am. Bull.*, 91:44–54.

Tracey, J. I., Jr., Sutton, G. H., et al., 1971. *Init. Repts. DSDP*, 8: Washington (U.S. Govt. Printing Office).
Turekian, K. K., and Wedepohl, K. H., 1961. Distribution of elements in some major units of the Earth's crust. *Geol. Soc. Am. Bull.*, 72: 175–192.
Turner, D. R., and Whitfield, M., 1979. Control of seawater composition. *Nature*, 281:468–469.
Unruh, D. M., and Tatsumoto, M., 1976. Lead isotopic composition and uranium, thorium, and lead concentrations in sediments and basalts from the Nazca Plate. *In* Yeats, R. S., Hart, S. R., et al., *Init. Repts. DSDP*, 34: Washington (U.S. Govt. Printing Office), 341–347.
van Andel, T. H., Heath, G. R., et al., 1973. *Init. Repts. DSDP*, 16: Washington (U.S. Govt. Printing Office).
Varnavas, S. P., Moorby, S. A., and Cronan, D. S., 1983. Partition geochemistry of sediments from Holes 506 and 509B, Deep Sea Drilling Project Leg 70. *In* Honnorez, J., Von Herzen, R. P., et al., *Init. Repts. DSDP*, 70: Washington (U.S. Govt. Printing Office), 297–302.
Veizer, J., and Compston, W., 1974. $^{87}Sr/^{86}Sr$ composition of sea water during the Phanerozoic. *Geochim. Cosmochim. Acta.*, 38:1461–1484.
Vidal, P., and Clauer, N., 1981. Pb and Sr isotopic systematics of some basalts and sulfides from the East Pacific Rise at 21°N (project RITA). Earth Planet. Sci. Lett., 55:237–246.
von Damm, K. L., Grant, B., and Edmond, J. M., 1983. Preliminary report on the chemistry of hydrothermal solutions at 21° North, East Pacific Rise. *In* Rona, P. A., Boström, K., Laubier, L., and Smith, K. L. (Eds.), *Hydrothermal Processes at Seafloor Spreading Centers*: New York (Plenum), pp. 369–389.
von der Borch, C. C., Nesteroff, W. D., and Galehouse, J., 1971. Iron-rich sediments cored during Leg 8 of the Deep Sea Drilling Project. *In* Tracey, J. I., Jr., Sutton, G. H., et al., *Init. Repts. DSDP*, 8: Washington (U.S. Govt. Printing Office), 829–835.
von der Borch, C. C., and Rex, R. W., 1970. Amorphous iron oxide precipitates in sediments cored during Leg 5, Deep Sea Drilling Project. *In* McManus, D. A., Burns, R. E., et al., *Init. Repts. DSDP*, 5: Washington (U.S. Govt. Printing Office), 541–544.
Walsh, J. N., Buckley, F., and Barker, J., 1981. The simultaneous determination of the rare-earth elements in rocks using inductively coupled plasma source spectrometry. *Chem. Geol.*, 33:141–153.
Wedepohl, K. N. (Ed.), 1974. *The Handbook of Geochemistry* (Vol. II/5): Berlin (Springer-Verlag), Ch. 82.
Williams, D. L., Green, K., van Andel, T. H., Von Herzen, R. P., Dymond, J. R., and Crane, K., 1979. The hydrothermal mounds of the Galapagos Rift: observations with DSRV 'Alvin' and detailed heat flow studies. *J. Geophys. Res.*, 84:7467–7484.
Yamaguchi, M., Armstrong, R. L., Russell, R. D., and Slawson, W. F., 1977. Strontium and lead isotopic investigations of igneous rocks from the Mid-Atlantic Ridge: DSDP, Leg 37. *In* Aumento, F., Melson, W. G., et al., *Init. Repts. DSDP*, 37: Washington (U.S. Govt. Printing Office), 613–616.
Yeats, R. S., Hart, S. R., et al., 1976. *Init. Repts. DSDP*, 34: Washington (U.S. Govt. Printing Office).
Zindler, A., Jagoutz, E., and Goldstein, S., 1982. Nd, Sr and Pb isotopic systematics in a three-component mantle: a new perspective. *Nature London*, 298:519–523.

Date of Initial Receipt: 13 August 1984
Date of Acceptance: 28 December 1984

APPENDIX
Sample Preparation and Analysis

Reagents and Standards

All reagents were certified reagent grade chemicals except for the acetic acid and hydrochloric acid used in sample dissolution; the latter were ULTREX (ultrapure) grade. Distilled and deionized water (18 mega-ohm) was used as solvent and dilutant. Readymade 1000-ppm stock standards from BDH Chemicals and J. T. Baker Chemicals were used for preparing the required working standards for analysis by atomic absorption spectrophotometry (AAS). Three standards were prepared for each element. The standard solutions were made up to match the sample solutions obtained by each of the three decomposition methods described below.

Sample Preparation

Each sample was dried overnight at 106°C, and, as in all subsequent weighings, the sample's weight was taken after a constant weight value was attained. The sample was then placed in a beaker with 250 ml of distilled water, stirred for 1 hr., filtered through a previously weighed filter, and washed with distilled water until the test for Cl^- failed (i.e., no precipitation after a drop of filtrate was added to 5% $AgNO_3$ solution). The sample was then washed several times with distilled–deionized water. The residue was dried at 106°C and weighed again. The weight loss of the sample should represent approximately the amount of salt present in the sediment.

The residue was powdered in an agate mortar and weighed. The sample was placed in a beaker and leached with slowly added, 10% acetic acid. The amount of acid used was that theoretically required to dissolve the carbonate in a sample of 100% $CaCO_3$, plus a small excess. This procedure was called "the first leach." After reaction ceased, the beaker's contents were stirred for ≈4 hr. and filtered through a previously weighed filter. The residue was thoroughly washed several times with distilled–deionized water (at least 500 ml of water were used) until the reaction for Ca^{2+} (a drop of filtrate on a Pt wire then placed in a flame) was very slight. The residue, considered to represent the carbonate-free fraction, was dried at 106°C, weighed, and powdered in an agate mortar. Two subsamples of 250 mg each were then weighed for further analysis.

The next selective chemical attack was termed "the second leach." An excess of mixed acid-reducing agent, consisting of hydroxylamine hydrochloride and acetic acid (1 M $NH_2OH \cdot HCl$ and 25% acetic acid), was then added to a 250-mg sample and stirred for ≈3 hr. The residue was filtered using a previously weighed filter and distilled–deionized water, dried, and weighed. The loss of weight should represent approximately the fraction of reducible, amorphous ferromanganese and manganese oxides (we found that the second leach also removed a portion of the minor phosphatic phase commonly present in our samples). The leachate was then transferred to a beaker and evaporated. At the end of evaporation, concentrated HNO_3 was added in order to destroy excess reducing agent. The solution was then cooled, diluted, and transferred via a volumetric flask to a plastic bottle.

The residue after the second leach was powdered (two samples of about 200 mg) and subjected to "the third leach." The sample material was placed in a beaker, treated with excess HCl (1 + 1 volume:volume), stirred, and heated for ≈3 hr. (hot plate temperature ≈180°C). The sample was filtered through previously weighed paper, washed, dried at 106°C, and weighed. The weight loss represents approximately the fraction of well-crystallized oxides. The leachate was transferred to a beaker, evaporated, diluted, and then transferred via a 100-ml flask to a plastic bottle. The analytical results for the two subsamples subjected to the third leach were always averaged. In Table 1B, the Pb and Sr data for the noncarbonate nonresidue fraction represent the sum of the second and third leachates.